“Impact of Quantum Mechanical Correction in Surface Potential based Compact Model on the Drain Current of nanoscale MOSFETs”

By

Siddiqa Sumaia

Nusrat Haque

Marzana Mantasha Mahmud

Submitted to the

Department of Electrical & Electronic Engineering

East West University

In partial fulfillment of the requirements for the degree of

Bachelor of Science in Electrical & Electronic Engineering

(B.Sc in EEE)

Spring 2011

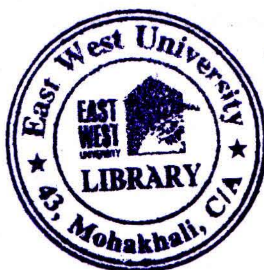

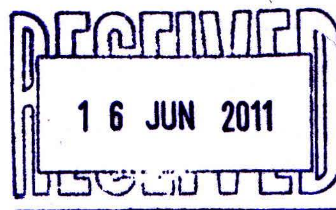

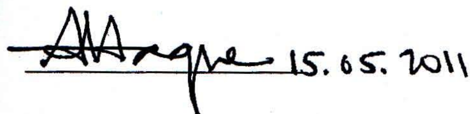

Thesis Advisor

Dr. Anisul Haque

Chairperson

Dr. Anisul Haque

ABSTRACT

Impact of the Quantum Mechanical (QM) correction in surface potential based compact model on the drain current of nanoscale MOSFETs is studied. We have considered a QM correction model to the surface potential (ψ_s) based compact model of M. A. Karim and A. Haque which has been proposed recently. This model does not use the bandgap widening approach. It directly adds the correction term to the semiclassical ψ_s. It accounts for the wave function penetration effect into the gate dielectric. The validity of this model has been demonstrated through the modeling of the gate $C - V$ characteristics. In our work we have studied the effect of this correction on the drain current characteristics of nanoscale MOSFETs. The results have been compared with two other models, PSP and Prégaldiny et al. both these methods incorporate QM correction through the bandgap widening approach. QM correction to ψ_s in PSP is derived from triangular well approximation while Prégaldiny uses the variational approach. When the wave function penetration effect is considered for a given semiconductor charge density the average distance of charges from the Si-gate oxide interface considering the QM effect is reduced. This leads to the lowering of ψ_s also. So the models neglecting the wave function penetration effect tend to overestimate the ψ_s. Hence both PSP and Prégaldiny which overestimate ψ_s tend to underestimate the drain current. The Karim model shows higher current than the two existing models and predicts a lower, more accurate threshold voltage. The percentage deviation of the drain current of the QM corrections of the PSP and Prégaldiny models has been observed with respect to Karim model. The percentage deviation is around 10 - 50% at higher gate voltage but the situation is extreme around 80 - 90% in moderate inversion ($V_{GS} \sim V_T$) whose effect is more pronounced. Comparison between them shows that the wave function penetration effect into the gate dielectric plays an important role in modeling the drain current of nanoscale MOSFETs.

Acknowledgements

We would like to thank Dr. Anisul Haque, Professor and Chairperson, Department of Electrical and Electronic Engineering (EEE), East West University (EWU), Dhaka, our supervisor, for his constant guidance, supervision, constructive suggestion and constant support during this thesis.

We are grateful to Muhammed Ahosan ul Karim, PhD. student, UC Berkeley and former Research Lecturer, Department of EEE, EWU, S. M. Salauddin, former Research Lecturer, Department of EEE, EWU, Tahseen Kamal, Senior Lecturer, Department of EEE, EWU, Khondker Zakir Ahmed, Senior Lecturer, Department of EEE, EWU, and Mahmudur Rahman Siddiqui, Research Lecturer, Department of EEE, EWU, for their suggestions and help.

We also want to thank our parents and all of our friends for their moral support and helpful discussion during this work.

EWU, Dhaka Authors

April, 2011

Approval

The thesis titled "Impact of Quantum Mechanical Correction in Surface Potential based Compact Model on the Drain Current of Nanoscale MOSFETs" submitted by Siddiqa Sumaia (2007-2-80-018), Nusrat Haque (2007-2-80-029) and Marzana Mantasha Mahmud (2007-2-80-005), session Spring, 2011, has been accepted satisfactory in partial fulfillment of the requirement of the degree of Bachelor of science in Electrical and Electronic Engineering on April, 2011.

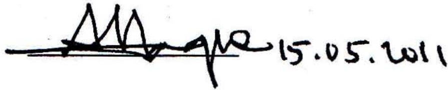

Dr. Anisul Haque

Professor and Chairperson

Department of Electrical and Electronic Engineering

East West University, Dhaka-1212, Bangladesh

Authorization Page

We hereby declare that we are the sole authors of the thesis. We authorize East West University to lend this thesis to other institution or individuals for the purpose of scholarly thesis.

(Siddiqa Sumaia)

(Nusrat Haque)

(Marzana Mantasha Mahmud)

We further authorize East West University to reproduce this thesis by photocopy or other means, in total or in part, at the request of other institutions or individuals for purpose of scholarly research.

(Siddiqa Sumaia)

(Nusrat Haque)

(Marzana Mantasha Mahmud)

Table of Contents

ABSTRACT ii

Acknowledgements iii

Approval iv

Authorization Page v

Table of Contents vi

List of Figures viii

Chapter 1 1

Introduction 1

1.1 Background 1

1.2 Literature Review 2

1.3 Objective 4

Chapter 2 5

Surface Potential Based Model 5

2.1 Appreciation of the Surface Potential Based Model 5

2.2 Effect of Gate-Substrate Voltage on Surface Condition 5

2.3 General relations in the region of inversion 9

2.4 Contacting the Inversion Layer 12

2.5 Surface Potential Based Drain Current Model 14

Chapter 3 18

Quantum Mechanical Effects 18

3.1 Energy quantization in the substrate due to quantum mechanical effects 18

3.1.1 Threshold Voltage shift 20

3.1.2 Increase in surface potential 20

3.2 Approaches to account for Quantum Mechanical Effects 20

3.2.1 Calculation of quantization in MOS inversion layer 21

3.2.2 Bandgap Widening Approach 24

Chapter 4 26

Quantum Mechanical Correction Model to the Surface Potential of Nanoscale MOSFETs 26

4.1 Basic approach of the Karim and Haque QM model 26
4.2 Derivation of the mathematical expression of the proposed QM model 28
Chapter 5 30
Results and Discussion 30
5.1 Results 30
5.2 Discussions 40
Chapter 6 41
Summary 41
6.1 Conclusion 41
6.2 Future work 42
References 43

List of Figures

Fig. 2.1 Two-terminal MOS under gate substrate biasing....6
Fig. 2.2 (a) A two terminal MOS with depletion (b) A two terminal MOS with inversion 8
Fig. 2.3 Surface potential vs. gate voltage....12
Fig. 2.4 Three terminal MOS structure, with n^+ region, biased at $V_{CB}(> 0)$ with voltages referred to the terminal C....13
Fig. 2.5 Surface potential vs. gate voltage with increasing V_{CB}....14
Fig. 2.6 A MOS transistor with terminal voltages referred to the source....15
Fig. 2.7 I_{DS} *vs* V_{DS} with increasing V_{GS}....17
Fig. 3.1 Electron density, n (z) as a function of distance from surface, z, for semiclassical and quantum-mechanical case....19
Fig. 3.2 Discrete energy levels due to quantization....19
Fig. 5.1 $\psi_s - V_{GS}$ characteristics....31
Fig. 5.2 $\psi_s - V_{GS}$ characteristics....33
Fig. 5.3 $I_{DS} - V_{GS}$ characteristics for calculating threshold voltages for the three models. ..35
Fig. 5.4 $I - V$ characteristics for $N_{sub} = 10^{17}\text{cm}^{-3}$ and $t_{ox} = 2.5$ nm, $W/L = 5$, $C_{ox} =$ 0.0138 F/cm^{-2}....36
Fig. 5.5 Comparison of the % deviation in drain current for $N_{sub} = 10^{17} cm^{-3}$....37
Fig. 5.6 : $I - V$ characteristics, here $N_{sub} = 10^{18} cm^{-3}$ and $t_{ox} = 1.5$ nm, $W/L = 5$, $C_{ox} = 0.023$ F/cm^{-2}....38
Fig. 5.7 Comparison of the % deviation in drain current for $N_{sub} = 10^{18} cm^{-3}$....39

Chapter 1

Introduction

From the time of its introduction in the 1960s, MOS transistor technology has been subject to incessant decrease in transistor dimensions and consequential progress in performance. The diminution of transistor dimensions has allowed for an exponential increase with time in the number of components per chip and its operational speed. Thus, with the growth in circuit complexity the use of computer-aided simulation tools called circuit simulators has become essential. Circuit simulators allow the circuit designer to predict and optimize circuit behavior before the circuit is realized in silicon. They are used to optimize circuit performance, verify the timing and functionality of circuits. Circuit models describing the terminal properties of the device of semiconductor devices that can be employed in circuit simulators are called compact models. The properties of the devices in compact models are either defined by means of a simplified set of equations or by an equivalent circuit model. In order to evaluate the performance of integrated circuits containing a large quantity of transistors, often several millions, compact transistor models are needed. Only in recent times, as device technology progresses into the deep submicron regime, with higher semiconductor substrate doping and high surface electric fields, Quantum Mechanical (QM) effects have become a significant part of modern devices. Therefore it is necessary to include QM effects in compact transistor models as well.

1.1 Background

With continual scaling of CMOS technology classical physics is insufficient to explain the behavior of a MOSFET. For modern device physics, where the metal-oxide-semiconductor (MOS) devices are down-scaled to the nanometer regime, QM effects have become an essential part. To obtain high density integration for MOS devices, it is necessary to reduce the gate oxide thickness and increase the substrate doping concentration. This results in a narrow and deep potential well. Electrons get confined at the semiconductor-insulator interface and it becomes necessary to take QM effects into consideration. In the state-of-the-

art MOSFETs due to increased vertical electric field the carrier energy quantization has become significant. The energy quantization and the shift of the inversion charge centroid delays the formation of inversion charge (threshold voltage (V_{th}) shift) and reduces the current driving capability (increase the effective oxide thickness). QM effects also result in an increase in the magnitude of ψ_s for a given gate voltage.

With the increasing importance of QM effects, many universities and institutions have developed QM simulators in order to predict these effects precisely. An accurate, self-consistent QM simulator is necessary in order to have a good understanding of these effects.

At this point, we differentiate between two categories of device models namely numerical device simulation models and compact models. Numerical device simulators are used to study the device physics and to predict the electrical, optical, and thermal behavior of a device. Numerical device simulators solve a set of partial differential equations associated with the physics involved in device operation. Their requirements of rigorous computation and huge amounts of memory prevent them from being used for circuit simulation. On the other hand, compact models describe the terminal properties of the device by means of a simplified computationally efficient set of equations or by an equivalent circuit model.

The Schrödinger and Poisson equations cannot be solved self-consistently at the device and circuit level simulation because of the huge computational cost. So, many researchers have tried to integrate QM effects into the classical models for device and circuit level simulation using empirical analytical expressions. This approach is termed as QM correction.

1.2 Literature Review

Just after the invention of modern silicon MOS transistor in 1960 its electrical characterization and dc current modeling began. The classical theory or strong inversion (SI) theory was then developed in 1964 [1], [2]. The SI theory considered only the drift component of the drain current. Then with the development of low power circuits, the below threshold or weak inversion (WI) mode of operation was explored [3], [4], [5]. WI models considered only the diffusion component of the drain current. The first MOSFET theory valid in all operating regions was the Pao-Sah drift-diffusion double-integral model [6]. The Pao-Sah model calculates the drain current as a double integral over the thickness of the inversion layer and the length of the channel. Because of the need for the numerical double integration,

it is not considered a compact model. However, the Pao-Sah equation is highly physical and still works as an ideal reference to test the accuracy of compact MOSFET models. Brews and Baccarani [7], [8] models based on surface potential as the key variable were established in 1978. The surface potential based models required numerical calculations with high precision, so these models were not considered appropriate for compact modeling at that time. The threshold voltage (V_T) approach [9], [10] was being adopted for SPICE simulations. In the V_T-based approach separate solutions are available for different regions of MOSFET operation. The V_T-based models use mathematical smoothing functions to describe the transition between weak and strong inversion. Smoothing functions ensure continuity of the current and its derivatives with respect to bias at the transition points. So, the V_T-based models are not accurate enough to represent the moderate inversion region which is widely used in low supply voltage circuits. Regardless of their limitations V_T-based models have been well used for much circuit design work. BSIM4 [10] and MOS Model 9 [11] are modern versions of threshold voltage-based models.

Finally in 1980s compact one-equation for all-region models were introduced [12], [13] and [14]. Next generation MOSFET models can be classified into two groups based on the adopted key variable. One approach is to express the model outputs in terms of charge densities by calculating the density of the inversion charge at the two ends of the channel. Examples of inversion charge models are ACM [15], EKV [16], and BSIM5 [17].

Another modeling approach is to solve for the surface potential at the source and drain ends of the channel. The terminal charges, currents and derivatives are then calculated from the surface potentials. These models are called surface potential or ψ_s-based models [6], [8], [18]-[23]. Here both the drift and diffusion currents are expressed in terms of surface potential and then simply summed up. This gives accurate modeling of the moderate inversion layer. Examples of such models are PSP [24], MOS model 11 [20], and HiSIM [17].

Surface potential based compact models have become popular for sub 100 nm MOSFETs. However, these models are based on semi-classical analysis. QM effects are added to the surface potential based models separately as corrections. Several models have been proposed to incorporate QM effect in the surface potential. The desired QM corrections, which are to be incorporated in MOSFET compact models, should be computationally efficient and accurate over a large range of device parameters and biasing conditions. The essential physics of electrostatics under accumulation bias in QM correction to ψ_s have been incorporated into very few existing models. Most existing models incorporate QM corrections through the

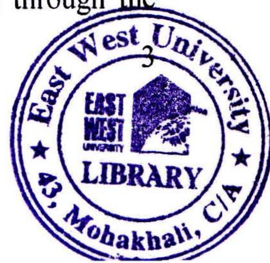

band-gap widening approach [25] which requires the modification of the underlying semiclassical model as well. In 2010, a different QM correction to the semiclassical surface potential approach was proposed [26]. It directly adds the QM correction term to semiclassical surface potential. The proposed model is a physically based model for QM corrections to the MOS surface potential. The model accounts for effect of wave function penetration within the proposed correction. This model proposes an explicit analytical expression of a QM correction term, $\delta\psi_s$, which has been directly added to the semiclassical surface potential. Since the proposed QM correction is not based on the band-gap widening model, it is not necessary to transform the semiclassical model. The validity of this model has been shown through the simulations of gate $C-V$ characteristics and has been compared with those of the other existing QM correction models [27], [28] for a variety of device parameters.

1.3 Objective

A number of works have explained the fundamental changes in the carrier distribution induced by the quantization effect. In order to understand how the performance of a MOSFET is affected by quantum mechanical effects, it is needed to extend this physical analysis into MOSFET voltage and current models for device and circuit design. Therefore, it is necessary to incorporate quantization analysis in the capacitance-voltage $(C-V)$and current-voltage $(I-V)$ characteristics. The Karim model of [26] is a physically based model for QM corrections to the MOS surface potential. The usefulness of this model has been illustrated through gate $C-V$ characteristics of a number of different MOS devices. The objective of this thesis is to analyze how the QM correction of [26] affects the modeling of the drain current, $I-V$ characteristics, of nanoscale MOSFETs. Comparisons will also be made with results obtained from a few other existing models for QM correction in ψ_s based models.

Chapter 2

Surface Potential Based Model

"Surface potential (ψ_S) is the total potential drop across the region from the surface to a point in the bulk outside the region". In MOS literature the top surface of the semiconductor is commonly referred to "the surface" [1]. ψ_S, the potential at the Si/SiO_2 interface is an implicit function of the terminal voltages.

2.1 Appreciation of the Surface Potential Based Model

It is desired to increase the physical content of the compact model and hence making it more suitable for modeling advanced MOS devices (where traditional compact models are not compatible with the circuit design). This has driven the switching from the threshold voltage-based (V_T) [9], [10] to surface-potential-based (ψ_S) approach [6], [8], [18]-[23]. The ψ_S based approach provides significant advantage in the development of compact models. One important benefit is that it allows one to increase the physics content of the model without sacrificing computational efficiency. Further, surface potential is a physically meaningful variable. Using the ψ_S based approach, a single expression valid in all regions of the MOSFET operation can be derived. All the compact ψ_S based MOSFET models are based on the charge-sheet approximation [8], [29] justified by comparison with the Pao-Sah double integration formula [6].

2.2 Effect of Gate-Substrate Voltage on Surface Condition

Our discussion begins by considering the two- terminal MOS, also known as the MOS capacitor, as shown in Fig. 2.1. The gate terminal has been connected to the body terminal. In doing so contact potential develops in going from the gate through the external connection to the bulk. So, even in the absence of external bias, the contact potential causes a net concentration of charges (usually positive) in the substrate. Another cause of this charge concentration is the "parasitic" charges (denoted by Q_0) that exist within the oxide and oxide-semiconductor interface. An external voltage (φ_{MS}) can be applied between the gate

and bulk to keep the semiconductor neutral and cancel the effects of the contact potential. This voltage is known as the flat-band voltage V_{FB}.

$$V_{FB} = \varphi_{MS} - \frac{Q_0}{C_{ox}} \tag{2.1}$$

where, C_{ox} is the capacitance between the two ends of the oxide

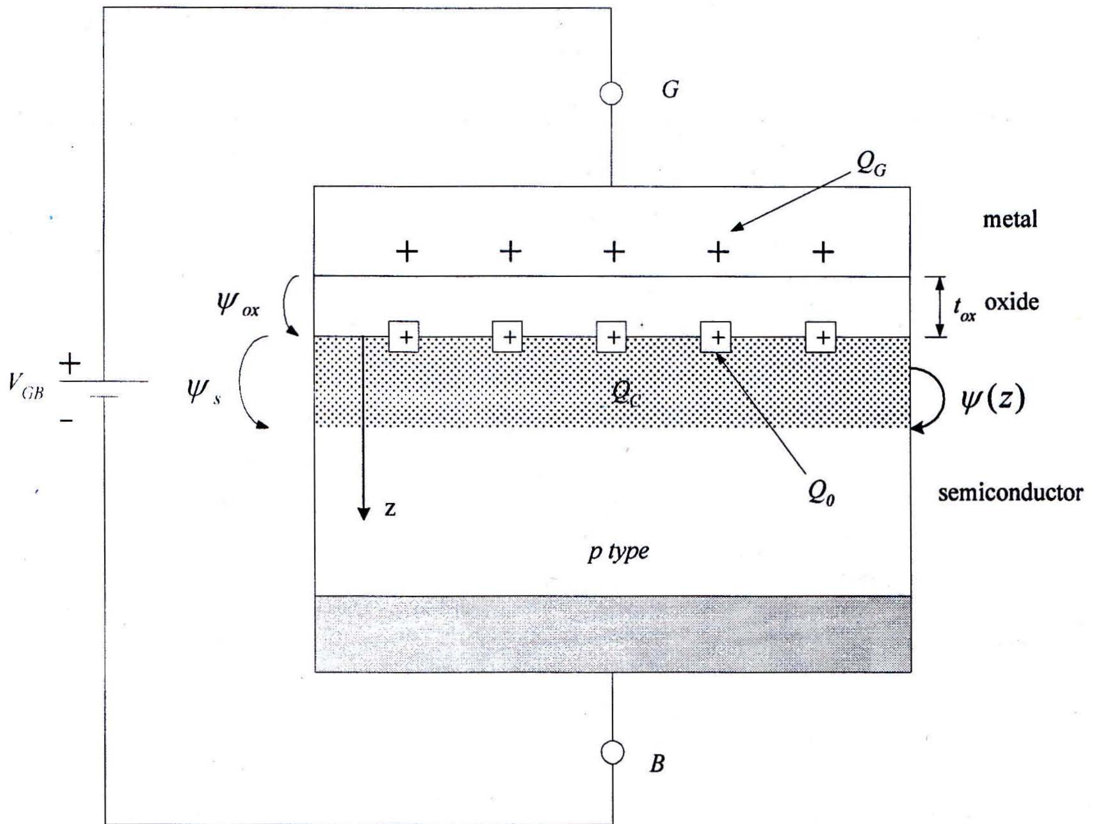

Fig.2.1 Two-terminal MOS under gate substrate biasing

When a voltage is applied externally, from gate to substrate, V_{GB} , then depending on the magnitude of V_{GB}, whether it is equal to, greater than and less than the flat band voltage V_{FB}, flat-band condition, accumulation, depletion and inversion occurs.The inversion region is of importance to us and will be considered in the further sections of this chapter. This section discusses the effect on the substrate (p-type substrate) when the externally applied voltage V_{GB}, is greater than the flat-band voltage V_{FB}. V_{GB} causes charges to appear in the

semiconductor which will be contained in a region adjacent to top surface of the semiconductor. The potential drops are encountered in the loop as:

$$V_{GB} = \psi_{ox} + \psi_s + \varphi_{MS} \tag{2.2}$$

where, V_{GB} = voltage of the external source

ψ_{ox} = potential drop across the oxide

ψ_s = surface potential

Now considering the charges, which are balanced one another for the charge neutrality in the total system:

$$Q_G + Q_0 + Q_C = 0 \tag{2.3}$$

where, Q_G = The charge on the gate

Q_0 = The effective interface charge

Q_C = The charge in the semiconductor under the oxide

Equation (2.3) can be expressed in terms of charge per unit area,

$$Q_G' + Q_0' + Q_C' = 0 \tag{2.4}$$

When V_{GB} increases above V_{FB}, the total charge on the gate becomes more positive than that of the flat-band condition. To maintain charge neutrality the positive change in Q_G' must be balanced by a negative change in Q_C'. The positive change in V_{GB} is shared among ψ_s and ψ_{ox}. If V_{GB} is not considerably higher than V_{FB}, the positive potential at the surface with respect to bulk drives away the holes from the surface, leaving it depleted. This condition is known as depletion, shown in Fig. 2.2 (a). As V_{GB} is increased above V_{FB} the hole density keeps on decreasing quite below the doping concentration value N_A. With the continual increase in V_{GB} more acceptor atoms are uncovered. ψ_s becomes adequately positive to attract a significant number of electrons to the surface. Eventually with a sufficiently high V_{GB} the density of electrons exceeds the density of holes at the surface. This condition is called inversion, shown in Fig. 2.2 (b). The electron concentration at the surface to that in the bulk can be related by:

$$n_{surface} = N_A e^{(\psi_s - 2\varphi_F)/\varphi_t} \tag{2.5}$$

where, φ_F is the Fermi potential and φ_t is thermal voltage. $\psi_s = 2\varphi_F$ is the onset of strong inversion.

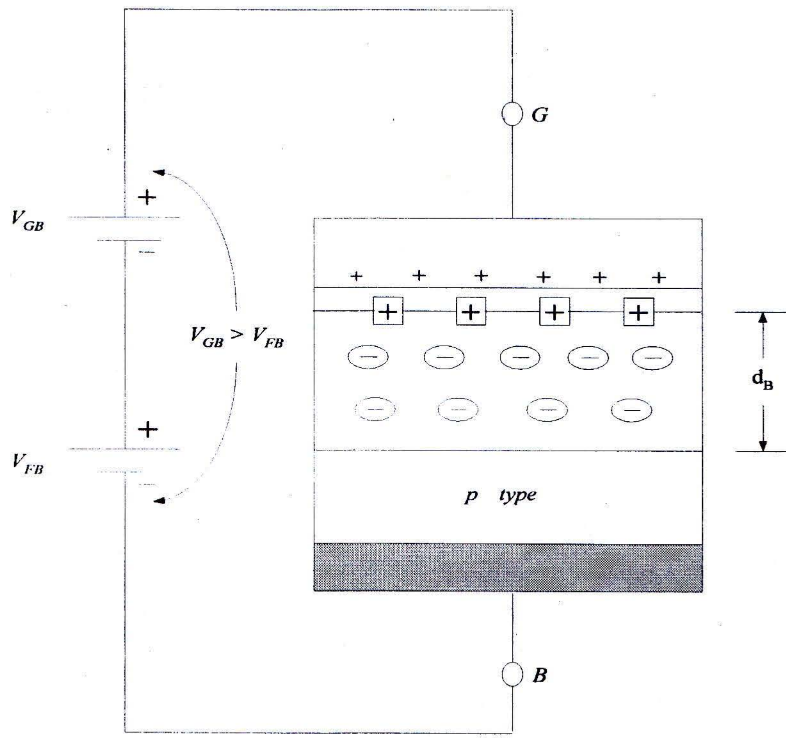

(a)

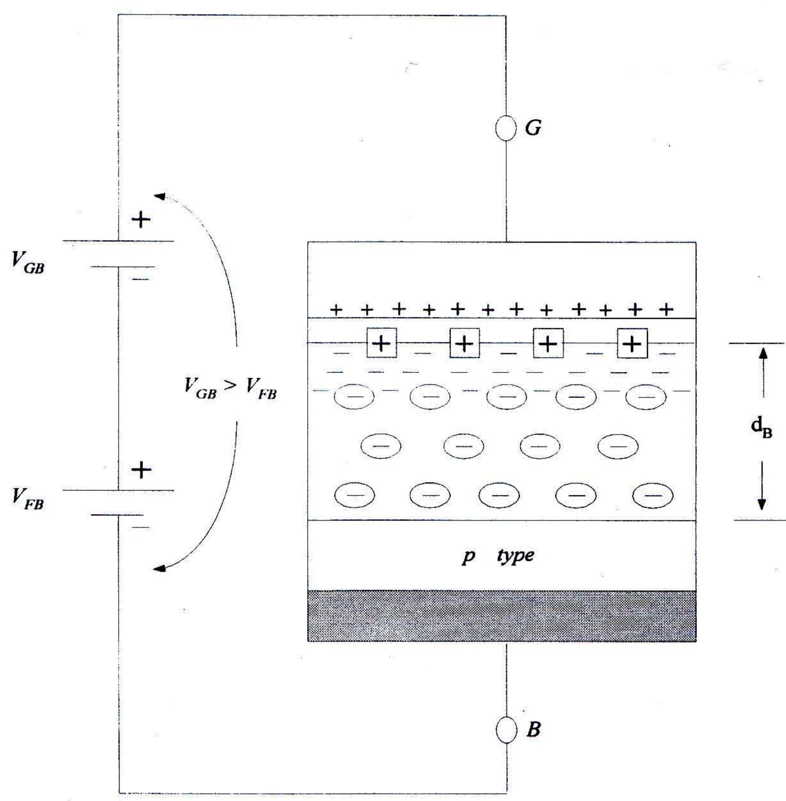

(b)

Fig.2.2 (a) A two terminal MOS with depletion (b) A two terminal MOS with inversion

2.3 General relations in the region of inversion

Considering a point z in the substrate in Fig. 2.1, $\psi(z)$ is the potential there with respect to the bulk, z direction is as shown in Fig. 2.1. The electron and hole concentrations can be found as follows:

$$n(z) = n_0 e^{\psi(z)/\varphi_t} \quad \text{and} \quad p(z) = p_0 e^{\Psi(z)/\varphi_t} \tag{2.6}$$

Generally both electrons and holes are present below the oxide, so the charge density can be expressed as:

$$\rho(z) = q[p(z) - n(z) - N_A] \tag{2.7}$$

From equations (2.6) and (2.7), Poisson's equation can be written as:

$$\frac{d^2\psi}{dz^2} = -\frac{q}{\epsilon_s}\left(p_0\, e^{-\psi_s/\varphi_t} - n_0\, e^{-\psi_s/\varphi_t} - N_A\right) \tag{2.8}$$

From these equations, for a given ψ_s, the values of $\psi(z)$, $n(z)$, $p(z)$, $\rho(z)$ and corresponding total charge per unit area in the substrate, Q'_C can be determined. From these relations the expression for Q'_C that can be derived is:

$$Q'_C = \mp\sqrt{2\, q\, \epsilon_s\, N_A}\sqrt{\varphi_t e^{-\psi_s/\varphi_t} - \psi_s - \varphi_t + e^{-2\varphi_F/\varphi_t}(\varphi_t e^{\psi_s/\varphi_t} - \psi_s - \varphi_t)} \tag{2.9}$$

This derivation has not been shown here. Here the – sign must be used for (depletion or inversion) and + sign for accumulation.

The charge per unit area above the oxide Q'_G is related to the potential across the oxide, ψ_{ox}, and the oxide capacitance per unit area, C'_{ox}, by :

$$Q'_G = C'_{ox}\psi_{ox} \tag{2.10}$$

In inversion where $\psi_s \geq \varphi_F$ equation (2.9) can be approximated as:

$$Q_C' = \mp\sqrt{2\, q\, \epsilon_s\, N_A}\sqrt{\psi_s + \varphi_t e^{(\psi_s - 2\,\varphi_F)/\varphi_t}} \tag{2.11}$$

The total charge per unit area below the oxide is the sum of the charges due to electrons in the inversion layer, Q_I' and the ionized acceptor atoms in the depletion region, Q_B' , that is ,

$$Q_C' = Q_I' + Q_B' \tag{2.12}$$

The depletion region can be defined by a sharp boundary, d_B , below the surface. The inversion layer is on top of this region. Normally, the depth of this region is much larger than the inversion layer, and hence the inversion layer is usually approximated to be a layer of charges of negligible thickness. This is called charge sheet approximation. So, all of the surface potential, ψ_s is assumed to be dropped across the depletion region.

The depletion region boundary is:

$$d_B = \frac{\sqrt{2\epsilon_s}}{qN_A}\sqrt{\psi_s} \tag{2.13}$$

The charge per unit area in the depletion region due to the uncovered acceptor atoms is:

$$Q_B' = -\sqrt{2q\, \epsilon_s N_A}\sqrt{\psi_s} \tag{2.14}$$

From equations (2.11), (2.12) and (2.14), the inversion charge per unit area is:

$$Q_I' = -\sqrt{2\, q\, \epsilon_s N_A}\left(\sqrt{\psi_s + \varphi_t e^{(\psi_s - 2\varphi_F)/\varphi_t}} - \sqrt{\psi_s}\right) \tag{2.15}$$

From charge neutrality we have,

$$Q_G' + Q_0' + Q_I' + Q_B' = 0 \tag{2.16}$$

Using the above equations a relation between V_{GB} and ψ_s can be derived as follows:

From (2.2), $V_{GB} = \psi_{ox} + \psi_s + \varphi_{MS}$

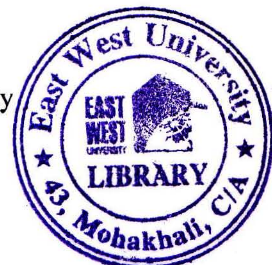

$$V_{GB} = \frac{Q'_G}{C'_{ox}} + \psi_s + V_{FB} + \frac{Q'_0}{C'_{ox}}$$

$$V_{GB} = \psi_s + V_{FB} + \frac{Q'_0 + Q'_G}{C'_{ox}} \tag{2.17}$$

From (2.16),

$$Q'_G + Q'_0 = -(Q'_I + Q'_B) \tag{2.18}$$

Both the inversion layer and depletion region charge is related to the potential across the region:

$$Q'_I = Q'_I(\psi_s) \text{ and } Q'_B = Q'_B(\psi_s) \tag{2.19}$$

Using equations (2.18) and (2.19), we have,

$$V_{GB} = \psi_s + V_{FB} - \frac{Q'_I(\psi_s) + Q'_B(\psi_s)}{C'_{ox}} \tag{2.20}$$

Finally using equations (2.11), (2.12) in (2.20), we get a relation between V_{GB} and ψ_s

$$V_{GB} = V_{FB} + \psi_s + \gamma\sqrt{\psi_s + \varphi_t e^{(\psi_s - 2\varphi_F)/\varphi_t}} \tag{2.21}$$

where, $$\gamma \equiv \frac{\sqrt{2\, q\, \epsilon_s N_A}}{C'_{ox}}$$

A typical surface potential vs. gate voltage characteristic has been shown in Fig. 2.3 where $\psi_s = \varphi_F$ and $\psi_s = 2\varphi_F$ is the onset of weak inversion and strong inversion respectively. Strong inversion begins at a surface potential of $\psi_s = 2\varphi_F + \varphi_{Z0}$, where φ_{Z0} is several φ_t, its value depending on substrate doping and oxide thickness.

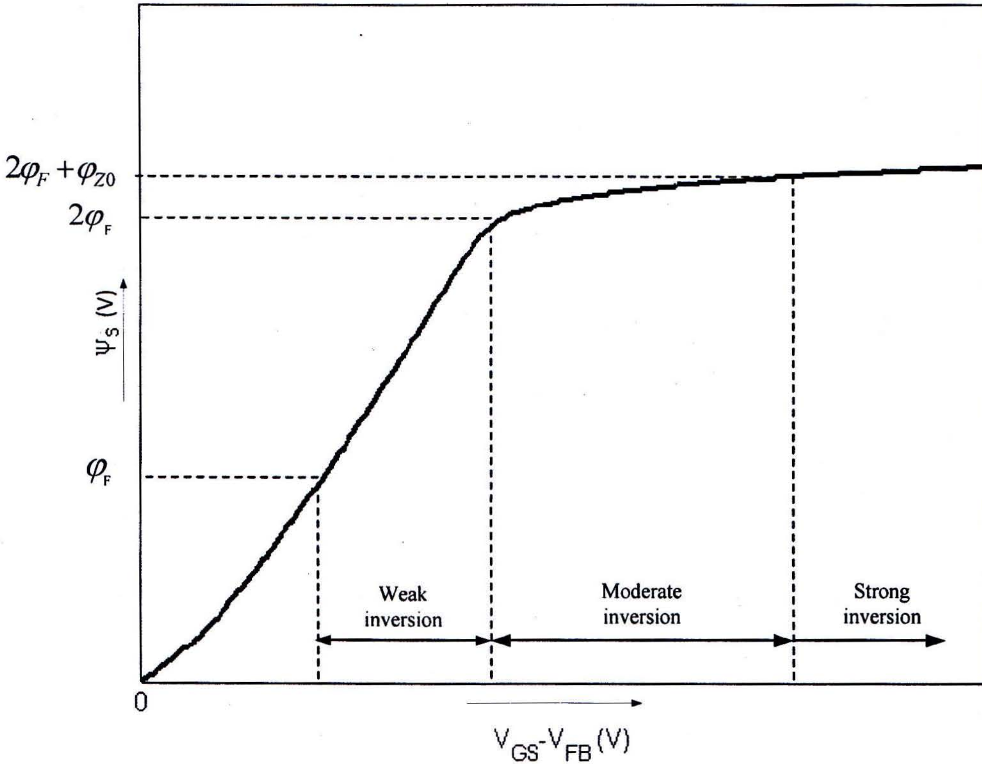

Fig.2.3 Surface potential vs. gate voltage

2.4 Contacting the Inversion Layer

Now a n^+ region is added to the basic two-terminal MOS structure. This is the three-terminal MOS structure. A n^+p junction is formed by this region and the substrate. The depletion region on the p side contains ionized acceptor atoms and the depletion region in then^+ region contains ionized donor atoms. Connection is made between the n^+ region terminal and the substrate terminal and a voltage source V_{CB} is placed as shown in Fig. 2.4. The value of V_{CB} is nonnegative to ensure that the n^+p junction is reversed biased. The gate and substrate terminals are also connected producing a surface potential ψ_s.

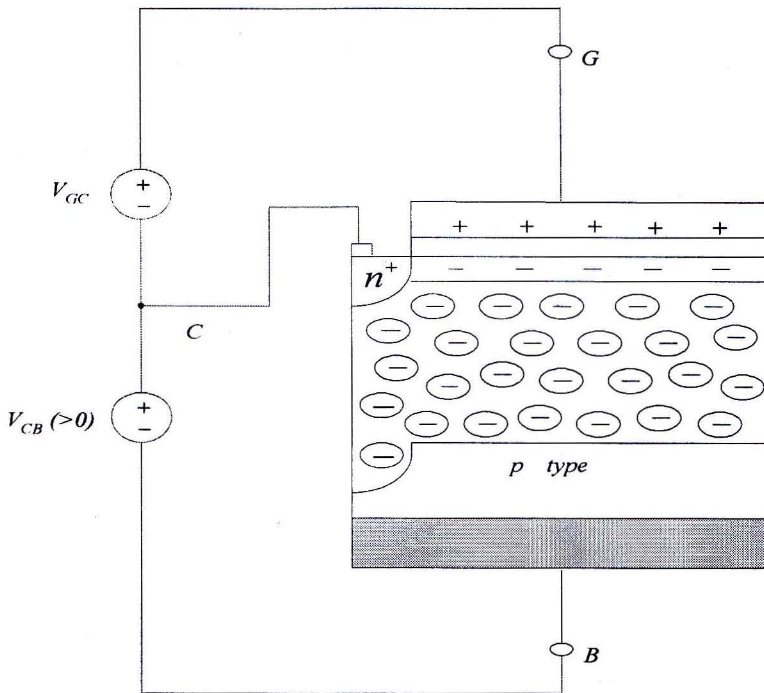

Fig.2.4 Three terminal MOS structure, with n^+ region, biased at $V_{CB}(> 0)$ with voltages referred to the terminal C

When $V_{CB} = 0$, for a certain V_{GB} a surface potential ψ_1, such that there is inversion, occurs. With the increasing value of V_{CB}, the region becomes more positive. Electrons are attracted from the inversion layer by this positive potential towards the n^+ region, and from it to the top terminal of the voltage source. With the rise in V_{CB}, depletion region under the n^+ region becomes wider and the inversion layer under the surface keeps decreasing. The inversion layer may also disappear if V_{CB} is quite large. So in order to bring back the surface to its original condition the surface potential must be increased the same amount the potential of the n^+ region increases. So, the surface potential must be increased from ψ_1 to $\psi_1 + V_{CB}$, as shown in Fig.2.5. This is achieved by increasing $V_{GB}$by an appropriate amount. Then the surface will be at the original level of inversion again. The electron concentration at the surface is fixed by $\psi_s - V_{CB}$. Thus the electron concentration at the surface to that in the bulk can be related by:

$$n_{surface} = N_A e^{[\psi_s - (2\varphi_F + V_{CB})]/\varphi_t} \tag{2.22}$$

Thus in order to increase the level of inversion ψ_s is counterbalancing against $2\varphi_F + V_{CB}$.

The relation between V_{GB} and ψ_s can be derived the same way as for the two-terminal structure, which is as follows:

$$V_{GB} = V_{FB} + \psi_s + \gamma\sqrt{\psi_s + \varphi_t e^{[\psi_s-(2\varphi_F + V_{CB})]/\varphi_t}} \tag{2.23}$$

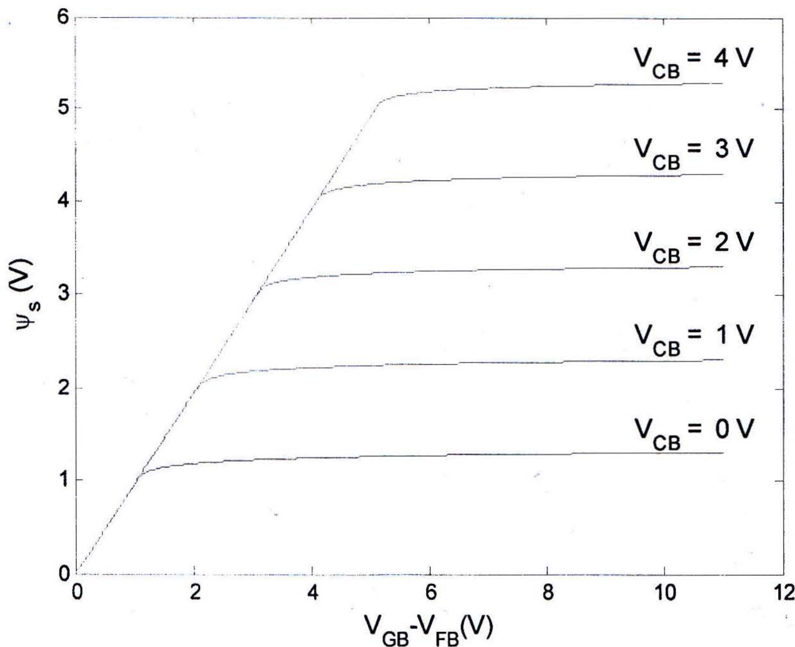

Fig.2.5 Surface potential vs. gate voltage with increasing V_{CB}

2.5 Surface Potential Based Drain Current Model

By adding one more terminal to the three-terminal MOS structure the inversion layer can be contacted at the opposite ends. When a voltage is applied between them, a current flows. In this section we will determine the drain current model based on the surface potential.
Throughout this section it is assumed that the channel is sufficiently long and wide, and the substrate is uniformly doped. The charge sheet approximation is also considered.

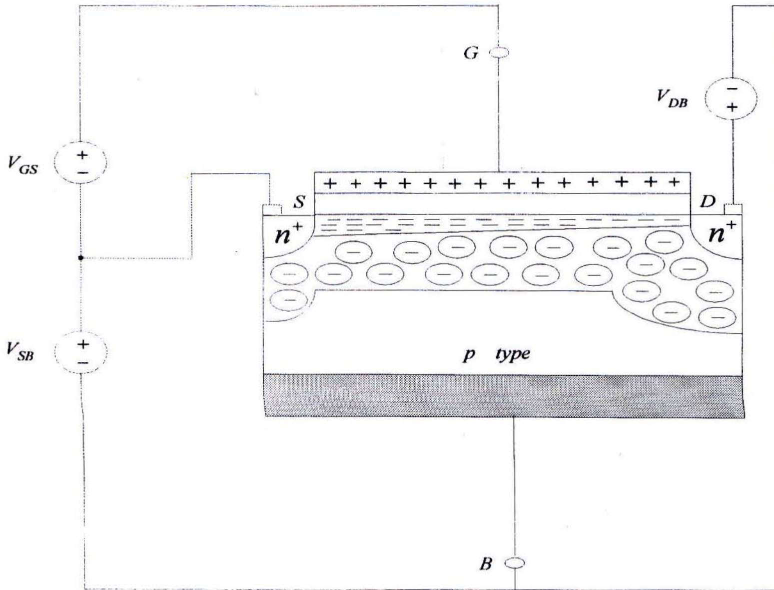

Fig.2.6 A MOS transistor with terminal voltages referred to the source

Connections are made as shown in Fig. 2.6. The contact potential, V_{CB} at the source end is replaced with V_{SB} . Similarly at the drain end of the channel V_{CB} is replaced by V_{DB}. Both pn junctions should be in reversed biased for emphasizing the normal operation of a MOS transistor.

When $V_{DB} = V_{SB}$, an electric field in the semiconductor, perpendicular to the surface is obtained. If $V_{DB} \neq V_{SB}$, a nonzero component of electric field in the horizontal direction appears. This is much smaller than the vertical component of electric field. So, the gradual channel approximation can be applied here, and only the vertical component of electric field is considered.

There are two components of the channel current, I_{DS}, the drift and diffusion current. Drift current, I_{DS1} occurs for the minority carrier's (electrons and holes) due to drift in the presence of the electric field. The diffusion current I_{DS2} occurs for the diffusion movement of charge.

$$I_{DS} = I_{DS1} + I_{DS2} \tag{2.24}$$

I_{DS1}due to presence of drift is,

$$I_{DS1} = \frac{W}{L}\int_{\psi_{s0}}^{\psi_{sL}} \mu(-Q_I')\, d\psi_S \tag{2.25}$$

I_{DS2} due to presence of diffusion is ,

$$I_{DS2} = \frac{W}{L}\varphi_t \int_{Q'_{IL}}^{Q'_{IL}} \mu \; dQ'_I \tag{2.26}$$

assuming μ is constant along the channel, we have:

$$I_{DS1} = \frac{W}{L}\; \mu \int_{\psi_{s0}}^{\psi_{sL}} (-\,Q'_I\,)\; d\psi_s \tag{2.27}$$

$$I_{DS2} = \frac{W}{L}\mu\varphi_t(Q'_{IL} - Q'_{I0}) \tag{2.28}$$

To evaluate I_{DS1} and I_{DS2}, Q'_I is need as a function of ψ_s which is

$$Q'_I \;=\; -\,C'_{ox}\left(V_{GB} - V_{FB} - \;\psi_s + \frac{Q'_B}{C'_{ox}}\right) \tag{2.29}$$

where,

$$Q'_B = -\mu C'_{ox}\sqrt{\psi_s} \tag{2.30}$$

Thus Q'_I becomes,

$$Q'_I = -C'_{ox}\big(V_{GB} - V_{FB} - \psi_s - \gamma\sqrt{\psi_s}\big) \tag{2.31}$$

Using equation (2.31) in (2.27), we get the drain current component due to the presence of drift as

$$I_{DS1} = \frac{W}{L}\; C'_{ox}\left[(V_{GB} - \; V_{FB})(\Psi_{sL} - \;\Psi_{s0}) - \frac{1}{2}(\Psi_{sL}^2 - \;\Psi_{s0}^2) - \frac{2}{3}(\Psi_{sL}^{3/2} - \;\Psi_{s0}^{3/2})\right] \tag{2.32}$$

Using equation (2.31) in (2.28), we get the drain current component due to the presence of diffusion as:

$$I_{DS2} = \frac{W}{L}C'_{ox}\left[\varphi_t\,(\psi_{sL} - \;\psi_{s0}) + \;\varphi_t\,\gamma\left(\psi_{sL}^{1/2} - \;\psi_{s0}^{1/2}\right)\right] \tag{2.33}$$

East West University EAST WEST UNIVERSITY LIBRARY 43, Mohakhali, C/A

ψ_{sL}, ψ_{s0} can be evaluated from the externally applied voltages, by replacing V_{CB} by V_{SB} at source end of the channel and V_{DB} at the drain end of the channel.

$$\psi_{s0} = V_{GB} - V_{FB} - \gamma\sqrt{\psi_{s0} + \phi_t e^{(\psi_{s0}-2\phi_F-V_{SB})/\phi_t}} \quad (2.34)$$

$$\psi_{sL} = V_{GB} - V_{FB} - \gamma\sqrt{\psi_{sL} + \phi_t e^{(\psi_{sL}-2\phi_F-V_{DB})/\phi_t}} \quad (2.35)$$

A typical $I - V$ characteristics obtained from the above equations has been shown in Fig. 2.7.

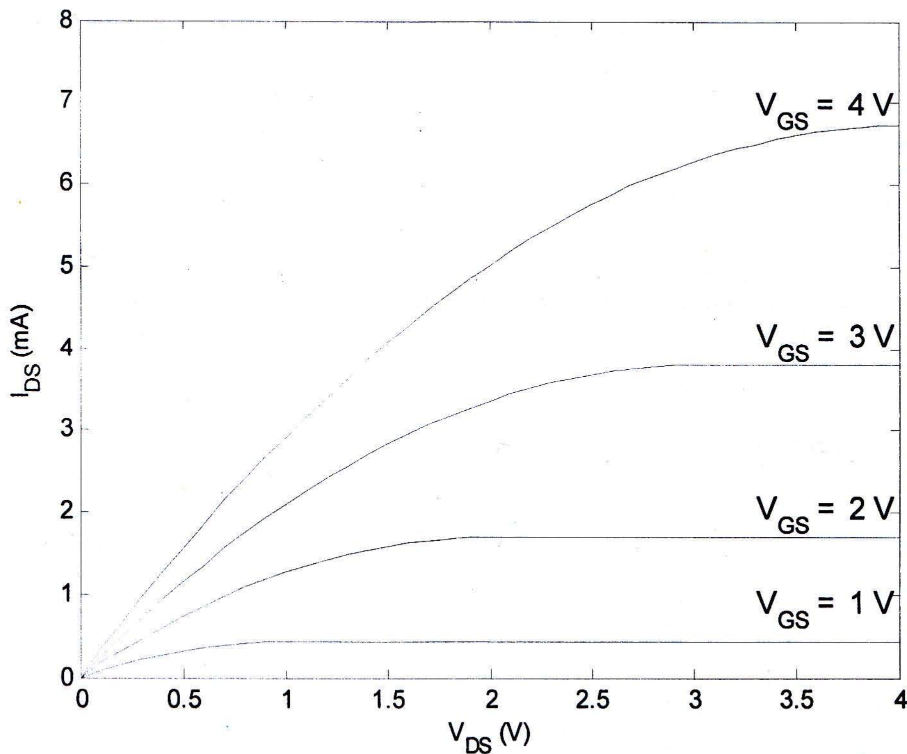

Fig.2.7 I_{DS} vs V_{DS} with increasing V_{GS}

Chapter 3

Quantum Mechanical Effects

As MOSFETs are continuously being scaled down, Quantum Mechanical Effects (QMEs) need to be considered [30]. It is important to account for the QMEs in the sub 90 nm designs of MOSFETs. Semiclassical models hence are inadequate and will lead to erroneous and misleading predictions of critical device structure and electrical behavior parameters such as the physical oxide thickness, threshold voltage, drive current, gate capacitance and sub-threshold swing. The major QMEs occurring in a MOSFET at deep sub-micron and the nanometer scales are the gate oxide tunneling, energy quantization in substrate and source to drain tunneling.

3.1 Energy quantization in the substrate due to quantum mechanical effects

The scaling down of MOS transistors is accompanied by both thinner oxides and more heavily doped channels, resulting in the increase in the transverse electric field at the silicon/silicon dioxide (Si/SiO_2) interface. Due to very high electric fields in the Si/SiO_2 the potential at the interface becomes steep. Under inversion condition, a potential well is formed by the oxide barrier and the silicon conduction band. Carriers in the inversion layer are confined in a narrow potential well. Because of the confinement of carrier motion in the direction normal to the surface, inversion-layer electrons must be treated quantum-mechanically as a two-dimensional (2D) electron gas [31]-[36], especially at high normal electric fields. The potential well is so narrow that the motion of the carriers of the surface channel is quantized in the direction perpendicular to the interface; consequently the carrier (probability) density is at a maximum inside the well and not at the boundaries, as shown in Fig. 3.1. Therefore, the operation of deeply scaled MOS transistors cannot be accurately described by semiclassical physics, accurate calculation of the inversion charge requires introducing concepts derived from quantum mechanics (QM).

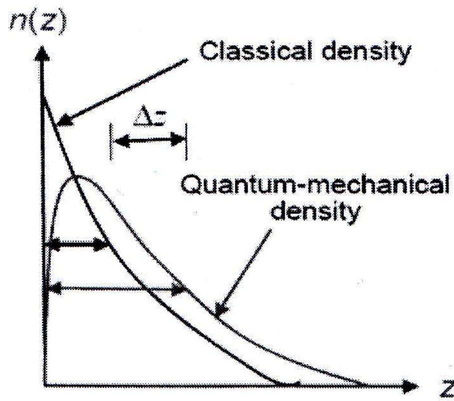

Fig.3.1 Electron density, n (z) as a function of distance from surface, z, for semiclassical and quantum-mechanical case

Due to confinement, the electron energies are quantized and hence the electrons occupy only the discrete energy levels [31]-[36]. This results in the electrons residing in some discrete energy levels, as shown in Fig. 3.2, which are above the classical energy level.

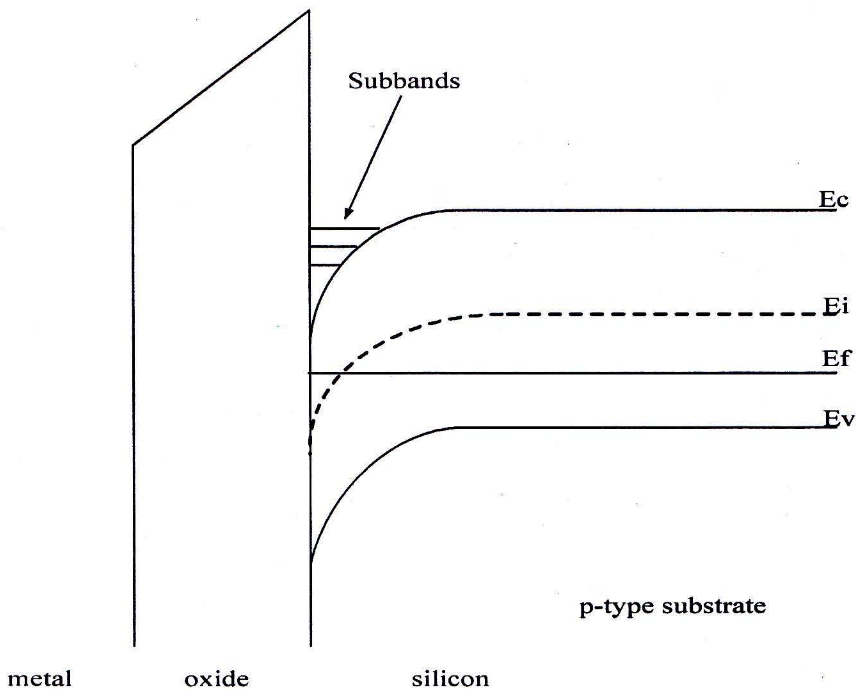

Fig.3.2 Discrete energy levels due to quantization.

3.1.1 Threshold Voltage shift

In the quantum theory the conduction band can no longer be regarded as a continuum of states, but rather splits into discrete subbands with a two-dimensional (2D) density of states. Because of the smaller density of states in the 2D system, the net sheet charge density of carriers in the channel is lower than that calculated from the classical case. Thus, it requires a larger gate voltage to generate the same charge sheet density. Consequently, the threshold voltage increases when energy quantization is considered [34], [37].

3.1.2 Increase in surface potential

The criterion for the onset of strong inversion is that the surface band bending reaches a value such that surface potential, $\psi_s = 2\varphi_F = \frac{2kT}{q}\ln\left(\frac{N_A}{n_i}\right)$. The semiclassical model says that the surface band bending $\psi_s$will be almost fixed at this value after inversion takes place since a slight increase in the surface potential results in a large buildup of electron density at the surface. For devices with gate oxides in the nanometer range, the surface band bending from the QM model is considerably larger than that from the classical model, for high electric field. This is because the 2-D carrier distribution of the subbands and discrete energy levels lead to a reduced charge density compared to semiclassical calculation. Therefore, an extra band bending is required for an increased charge density. This indicates the importance of considering QM effects for these devices with where the surface electric field is high. The models without considering the QM confinement effects will lead to errors in the evaluation of the surface potential versus the gate-voltage relationship.

3.2 Approaches to account for Quantum Mechanical Effects

Quantum mechanical effects modify the channel charge through two mechanisms:

i) The channel carriers get distributed among discrete energy levels instead of in a single energy band.

ii) The peak of the carrier concentration is located some distance away from the surface in the substrate, which is a result of superimposition of wave functions at the different energy levels.

3.2.1 Calculation of quantization in MOS inversion layer

The Schrödinger equation is a fundamental equation of quantum mechanics. The Schrödinger equation is related to another equation, the Poisson equation in semiconductor devices. These are both examples of second order partial differential equations. To model the quantum mechanical effects of quantum confinement, the self-consistent solution of the Schrodinger equation with Poisson's equation is required. The quantum mechanical calculation of inversion carriers is given by the solution of Schrödinger-Poisson's equations self-consistently.

The Poisson equation is given by:

$$\nabla^2 \psi(z) = -\frac{\rho(z)}{\epsilon_0} \tag{3.1}$$

The charge density $\rho(z)$ accounting for both electrons and holes below the oxide is as follows:

$$\rho(z) = e\,[\,p(z) - n(z) - N_A] \tag{3.2}$$

In Chapter-2 the electron and hole concentrations that have already been found. Equation (2.6) is substituted in equation (3.2) and equation (3.1). The Poisson equation can then be written as:

$$\frac{d^2\psi}{dz^2} = -\frac{e}{\epsilon_s}\,(\,p_0\, e^{-\psi(z)/\varphi_t} - n_0\, e^{-\psi(z)/\varphi_t} - N_A\,) \tag{3.3}$$

where, $\epsilon(z)$is the permittivity of the material.

The one-dimensional (1D), time-independent Schrödinger equation is given by:

$$\frac{d^2\zeta_i}{dz^2} + \frac{2m_3}{\hbar^2}[E_i + e\,\psi(z)]\zeta_i(z) = 0 \tag{3.4}$$

where, ζ_i is the wave function corresponding to the ith subband, m_3 is the normal effective mass and E_i is the eigenvalue corresponding to the ith subband.

Quantization in MOS inversion layer is calculated by solving Schrödinger and Poisson's equations self-consistently. The self-consistent calculation starts with an initial estimate for $\psi(z)$ and then solves equations (3.3) and (3.4).

A trial potential $\psi_1(z)$ is guessed for the iterative solution for Schrödinger-Poisson's equation and the Schrödinger equation is solved. From the obtained wavefunctions and their corresponding eigen energies, the carrier concentrations $n(z)$ is then calculated and is substituted into the charge part of the Poisson's equation. The potential derived from this is substituted back to Schrödinger's equation. Hence successfully the Schrödinger's equation and the Poisson's equation are being solved self-consistently until the output potential from equation (3.3) agrees with the input potential in equation (3.4) within specified limits.

The solution of Schrödinger-Poisson's equations is usually enough to provide necessary corrections to the semiclassical case. But from the circuit modeling point of view, solution of Schrödinger-Poisson equations is excessively complex and requires immense computational cost.

Stern first carried out the numerical self-consistent calculation for Si inversion layer [38]. It is required to obtain physically reasonable approximations for Schrödinger equation at the silicon dioxide interface. So self-consistent calculation made in [38] was based on three major approximations for the analysis of the electrical behavior of the MOS system:

i) The effective-mass approximation is valid.
ii) The envelope wave function, $\zeta(z)$, vanishes at the Si/SiO_2 interface
iii) The effects of surface states are neglected and the effect of any charges in the oxide adjacent to the semiconductor is replaced by an equivalent electric field.

The boundary conditions used by [38] for the solution of equation (4) are $\zeta_i(\infty) = 0$ and $\zeta_i(z)$ vanishes at the surface, where z = 0. This is a good approximation for the $Si\text{-}SiO_2$ interface.

The potential $\psi(z)$ which appears in (3.5) is the solution of the Poisson's equation:

$$\frac{d^2\psi}{dz^2} = -\left[\rho_{depl}(z) - e\sum_i n_i \zeta_i^2(z)\right]/k_{sc}\epsilon_0 \qquad (3.5)$$

Here, ϵ_0 is the permittivity of free space, k_{sc} is the dielectric constant of the semiconductor

andn_i is the carrier concentration in the i^{th}subband, given by:

East West University
EAST WEST UNIVERSITY
LIBRARY
43, Mohakhali, C/A

$$n_i = \left(\frac{n_{vi} m_{di} kT}{\Pi\hbar^2}\right) F_0[(E_F - E_i)/kT] \quad (3.6)$$

Here, $F_0(x) = \ln(1 + e^x)$, n_{vi} and m_{di} are the valley degeneracy and the density-of-states effective mass per valley, E_F is the Fermi energy and $\rho_{depl}(z)$ is the charge density of the depletion layer given by

$$\rho_{depl}(z) = -e(N_A - N_D), 0 < z < z_d$$

$$\rho_{depl}(z) = 0, \qquad z > z_d$$

$z_d$is the width of the depletion layer given by:

$$z_d = \sqrt{\frac{2k_{sc}\epsilon_0\psi_d}{e(N_A - N_D)}} \quad (3.7)$$

Here, k_{sc} is the dielectric constant of silicon, and $\psi_d$is the effective band-bending from the bulk to the surface, apart from the contribution of the inversion layer itself; its value is given by [38]

$$\psi_d = \psi_s - \frac{kT}{e} - \frac{eN_{inv}z_{av}}{k_{sc}\epsilon_0} \quad (3.8)$$

where $\psi_s$is the total band bending from the bulk to the surface, $N_{inv} = \sum_i n_i$ is the inversion carrier density per unit area, z_{av} is the average penetration of the inversion carriers into the semiconductor from the oxide-semiconductor interface. The boundary conditions used to obtain the solution of Eq. (5) are:

$$\frac{d\psi}{dz} = 0 \text{ for } z = \infty$$

$$\frac{d\psi}{dz} = -F_s \text{ at } z = 0$$

where

$$F_s = \frac{e(N_{inv} + N_{depl})}{k_{sc}\epsilon_0} \quad (3.9)$$

and

$$N_{depl} = z_d(N_A - N_D) \quad (3.10)$$

N_{depl} is the carrier density per unit area in the depletion layer. In the self-consistent calculation made in [38], equations (3.4) - (3.10) are solved iteratively for a given value of N_{inv} until the profile converges within a specified limit. The calculation is started with a small value of N_{inv} and then increased gradually to larger values, taking the results of each case to construct the starting potential for the next. The results obtained are numerically self-consistent; however they cannot be incorporated into device simulators.

3.2.2 Bandgap Widening Approach

Modeling of the silicon bandgap at inversion conditions was introduced by van Dort [25] to account for quantization effects. This model uses the fact that energy quantization effectively increases the bandgap at the surface region of the substrate under the gate. The amount of the bandgap increase is related to the surface transverse field. By solving the Schrödinger equation within a triangular potential well the relationship between the bandgap change with the electric field can be determined.

At high doping levels, QM effects become dominant. A greater surface potential ($\psi_{s(QM)}$) is required than the conventional value of the surface potential (ψ_s).

$$\psi_{s(QM)} = \psi_s + \frac{\Delta\epsilon}{q} + F_s\,\Delta z \qquad (3.10)$$

In this equation, $\Delta\epsilon$ is the energy gap between the bottom of the conduction band and the first allowed energy level, F_s is the electric field perpendicular to the interface, and Δz the increase of the average distance to the interface compared to the classical solution.

where, $$\Delta z = < z_{(QM)} > - < z_{(sc)} >$$

and z is the coordinate perpendicular to the interface.

$$\Delta\epsilon \approx \beta\left(\frac{k_{sc}}{4qkT}\right)^{1/3} \max\,(E_1, 0)^{2/3}\,,$$ here β is a physical constant

where E_1 is the ground state energy.

Due to the splitting of the energy levels the bandgap becomes larger. The effect of displacement of electron distribution is incorporated through the third term in equation (3.10).

This term expresses the extra band bending required. The bandgap widening is proportional to the 2/3 power of the electric field perpendicular to the interface, F_S.

The proposed model modifies the bandgap in the inversion layer and the intrinsic carrier concentration in the inversion layer as follows:

$$E_{g(QM)} = E_g + \frac{13}{9}\Delta\epsilon \quad (3.11)$$

$$n_{i(QM)} = n_i exp^{(\Delta E_g/2kT)} \quad (3.12)$$

The advantage of this model is that it can be built in a device simulator. Although this model addresses the threshold voltage shift to the energy quantization, there are problems with the van Dort model. By making the bandgap as the function of surface electric field the profile of the channel carriers remains semiclassical, that is, the carriers are peaked at the Si/SiO_2 interface. Secondly, since charge is proportional to the amount of the bandgap increasing, it is proportional to $F_S{}^{2/3}$, implying that the gate capacitance which is the derivative of channel charge with respect to the gate bias, will suffer singularity at the flatband condition.

Chapter 4

Quantum Mechanical Correction Model to the Surface Potential of Nanoscale MOSFETs

The band-gap widening approach indirectly includes quantum mechanical (QM) correction. In the band-gap widening model, the proposed QM correction requires transformation of the semiclassical model. The existing physically based QM corrections are either derived from triangular well approximation or variational technique [38]. The physics of both approaches are dependable but none of the techniques are quantitatively correct. A physically based explicit analytical model for the QM correction to the surface potential of nanoscale MOS devices was proposed in [26]. The validity of the proposed model was shown through comparison with other existing analytical and numerical models with excellent agreement to published numerical data.

4.1 Basic approach of the Karim and Haque QM model

The Karim and Haque QM correction to the semiclassical surface potential (ψ_s), is valid for both n-channel MOS (nMOS) and p-channel MOS (pMOS) devices. This model directly adds the QM correction term to the semiclassical ψ_s, instead of applying indirect band-gap widening approach.

At the silicon-silicon dioxide (Si-SiO_2) interface, the inversion carriers are treated as a sheet of charge in the semiclassical charge sheet model. Due to QM effects the energies of the charge carriers under inversion bias get quantized. The sheet charge corresponding to the quantized charge carriers is shifted into Si by an amount z_{av}considering the QM effect. Here z_{av} is the average penetration of the inversion carriers into the semiconductor from the oxide-semiconductor interface. Due to this shift of the charge the magnitude of the surface potential due to the QM effect increases under both inversion and accumulation conditions. The correction to the surface potential due to the QM effect using the physics of the QM charge sheet model has been shown as

$$\delta\psi_s = -\frac{Q_{inv} z_{av}}{\epsilon_0\, \epsilon_{Si}} \tag{4.1}$$

where Q_{inv} is the inversion charge density. Whereas most existing surface-potential-based models (such as [24], [27], [28], [39] and [40]) use the band-gap widening approach of van Dort et al. [25] to incorporate QM correction to the semiclassical ψ_s .

The surface potential $\psi_{s(QM)}$ including the QM effect is expressed as:

$$\psi_{s(QM)} = \psi_{s(sc)} + \delta\psi_s \tag{4.2}$$

Here, $\psi_{s(sc)}$ is the semiclassical surface potential neglecting the QM effect, which can be be estimated from the well-known Pao–Sah equation [6] using the gradual channel and charge sheet approximations in a variety of ways.

The penetration of the wave function into the oxide increases with shrinking gate oxide thickness and increasing substrate doping concentration, [41]. Precise evaluation of the quantized eigen energy levels in the semiconductor region depends on the amount of this wave function penetration into the oxide region. The wave function cannot be forced to vanish at the oxide-semiconductor interface and has to be taken into account. The Airy function approximation provides a simple analytical expression for QM correction. According to the Airy function approximation, the energies of the quantized states are proportional to $F_{ox}^{2/3}$, where F_{ox} is the oxide electric field. In [42] it has been shown that the two-third power law is not accurate for the state of- the-art nanoscale MOSFETs, even when the wave function penetration effect into the gate dielectric is considered.

The energy of the lowest quasi- bound state E_1 expressed in [42] is as:

$$E_1 = \pm\zeta_1 \left(\frac{|F_{ox}|cm}{MV}\right)^{\lambda} \tag{4.3}$$

Here, $\zeta_1 = 77$ meV and $\lambda = 0.61$ for electrons, and $\zeta_1 = 88$ meV and $\lambda = 0.64$ for holes, incorporating the wave function penetration effect. The z_{av} is reduced when wave function penetration effect is taken into account for a given semiconductor charge density. Due to this the magnitude of ψ_s is also lowered. Therefore, in strong inversion and strong accumulation regions, the QM corrections which neglect the wave function penetration effect overestimate the magnitude of ψ_s .

Under the modified Airy function approach, z_{av} can be expressed as:

$$z_{av} = \frac{E_1}{qF_s} \tag{4.4}$$

where, F_s is the Si surface electric field.

4.2 Derivation of the mathematical expression of the proposed QM model

The inversion charge density is $Q_{inv} = Q_s - Q_b$. This can be written in the form:

$$Q_{inv} = -C_{ox}\left(V_g - V_{FB} - \psi_{s(QM)}\right) - Q_b \tag{4.5}$$

where $C_{ox} = (\epsilon_0 \epsilon_{Si}/T_{ox})$ is the oxide capacitance per unit area, V_{FB} is the flat-band voltage, $Q_b = \mp\gamma C_{ox}\sqrt{\psi_{s(QM)}}$ is the depletion charge density, and $\gamma = \sqrt{2q\,\epsilon_0\epsilon_{Si}N_{sub}}/\,C_{ox}$ is the body factor. Here, the (−) sign is for n-MOS devices, and the (+) sign is for p-MOS devices. An implicit equation for $\delta\psi_s$can be obtained by substituting equations (4.4) and (4.5) into equations (4.1) and using (4.2). Although the implicit equation can iteratively be solved, the numerical solution of the implicit equation is not pleasing from concern of computational efficiency.

$\delta\psi_s$ shows satisfactory convergence after the first two iterations, which has numerically been verified. So, considering only the first two iterations, an explicit analytical expression for $\delta\psi_s$ has been derived, which is as shown:

$$\delta\psi_s = \frac{C_{ox}\left[V_g - V_{FB} - \left(\psi_{s(sc)} + \delta\psi_s^1 \pm \gamma\sqrt{\left|\psi_{s(sc)} + \delta\psi_s^1\right|}\right)\right]E_1^1}{q\epsilon_0\epsilon_{ox}F_{ox}^1} \tag{4.6}$$

and $\delta\psi_s^1$, the first order solution is

$$\delta\psi_s^1 = \frac{C_{ox}\left[V_g - V_{FB} - \left(\psi_{s(sc)} \pm \gamma\sqrt{\left|\psi_{s(sc)}\right|}\right)\right]E_1^0}{q\epsilon_0\epsilon_{ox}F_{ox}^0} \tag{4.7}$$

Here, the (+) signs are for n-MOS devices, and the (-) signs are for p-MOS devices. E_1^0 and F_{ox}^0 are the zeroth-order terms, and E_1^1 and F_{ox}^1 are the first-order terms, respectively. These are given by:

$$E_1^0 = \zeta_1 \left(\frac{|F_{ox}^0| cm}{MV}\right)^{\lambda} \tag{4.8}$$

$$E_1^1 = \zeta_1 \left(\frac{|F_{ox}^1| cm}{MV}\right)^{\lambda} \tag{4.9}$$

$$F_{ox}^0 = \frac{C_{ox}[V_g - V_{FB} - \psi_{s(sc)}]}{\epsilon_0 \epsilon_{ox}} \tag{4.10}$$

$$F_{ox}^1 = \frac{C_{ox}[V_g - V_{FB} - (\psi_{s(sc)} + \delta\psi_s^1)]}{\epsilon_0 \epsilon_{ox}} \tag{4.11}$$

$\delta\psi_s$ is the main result which can be added to the semiclassical surface potential to attain QM corrected result. However it has been noted that due to the nature of equations (4.6) and (4.7), $\psi_{s(QM)}$ leads to diverging derivative with respect to the gate voltage at flat-band (V_{FB}). Through numerical verification it has been found that $\delta\psi_s$ negligible around the flat-band. The problem of diverging derivative has been overcome exploiting this observation. It has been done as follows:

$$\psi_{s(sc)} = \psi_{s(sc)}, \; V_{tr1} \leq V_g - V_{fb} \leq V_{tr2},$$

$$= \psi_{s(sc)} + \delta\psi_s, \quad otherwise. \tag{4.12}$$

Here, V_{tr1} and V_{tr2} are two transition voltages such that $V_{tr1} < 0$ and $V_{tr2} > 0$. Choices for $V_{tr1} = 0.001$ V and $V_{tr2} = 0.2$ V and, for p-MOS devices, $V_{tr1} = -0.15$ V and $V_{tr2} = 0.001$ V that work well for all cases. These values have been verified through numerical simulations for a large variety of substrate doping densities and channel voltages.

A notable feature of this proposed QM correction is that $\delta\psi_s$is independent of V_{CB}, $V_{CB}$is the channel voltage that appears due to non-zero drain voltage. V_{CB} affects only $\psi_{s(sc)}$.

Chapter 5

Results and Discussion

5.1 Results

In our work we have analyzed the impact of Quantum Mechanical (QM) correction to the surface potential based compact models on the drain current of nanoscale MOSFETs. As already discussed in the previous chapters, due to the scaling down of MOSFETs, the semi-classical models become inadequate and the QM effects need to be considered. We have computed the $I - V$ characteristics for two different sets of device parameters using the surface potential (ψ_s) based approach and incorporated the QM correction methods of PSP [24] and Prégaldiny [28] into it. Both these methods incorporate QM correction through the bandgap widening approach and neglect the wave function penetration effect. QM correction to ψ_s in PSP is derived from triangular well approximation while Prégaldiny uses the variational approach. Comparison has been made between these existing models with the Karim model [26] which addresses the effect of wave function penetration into the gate dielectric.

In order to maintain uniformity with the device parameters that have been considered in the proposed model [26] to validate the $C - V$ characteristics, we have chosen the same sets of data, that is, in the first case $N_{sub} = 10^{17}\text{cm}^{-3}$ and $t_{ox} = 2.5$ nm and in the second case $N_{sub} = 10^{18}\text{cm}^{-3}$ and $t_{ox} = 1.5$ nm .

In Fig. 5.1 comparison between the ψ_s vs V_{GS} characteristics according to the surface potential (ψ_s) based model, which is essentially semiclassical, and the QM correction incorporated model PSP [24], Prégaldiny [28] and Karim model [26] has been shown for the first case. Comparison of the models with the semiclassical results shows that the model of [24] and [28], which incorporate the QM correction to the surface potential through the band-gap widening approach, overestimates the ψ_s. The increase in the surface potential is more when a channel voltage (V_{CB}) is applied.

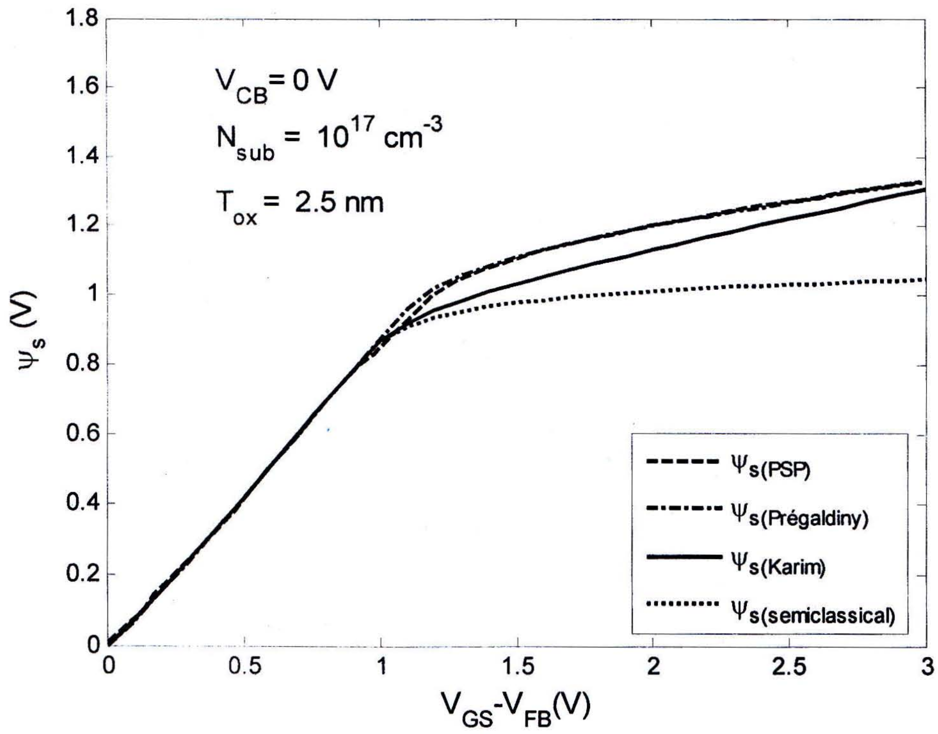

(a)

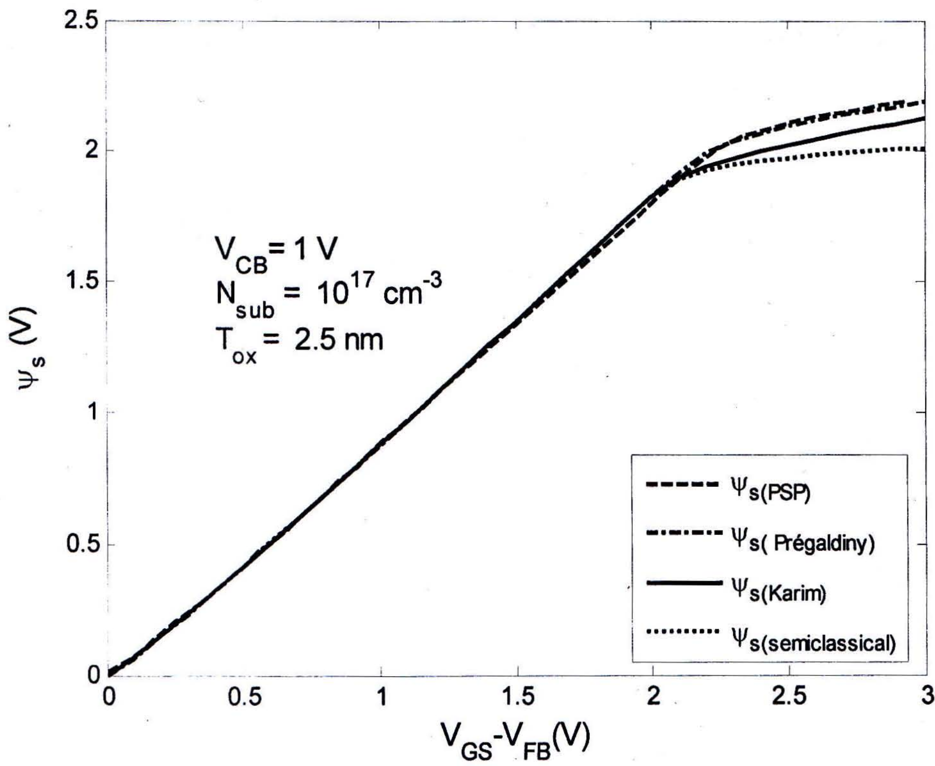

(b)

Fig.5.1 $\psi_s - V_{GS}$ characteristics

East West University LIBRARY 43, Mohakhali, C/A

Fig. 5.2 shows the comparison between the ψ_S vs V_{GS} for the second case. The existing models again tend to overestimate the surface potential, whereas the Karim model predicts the same more accurately.

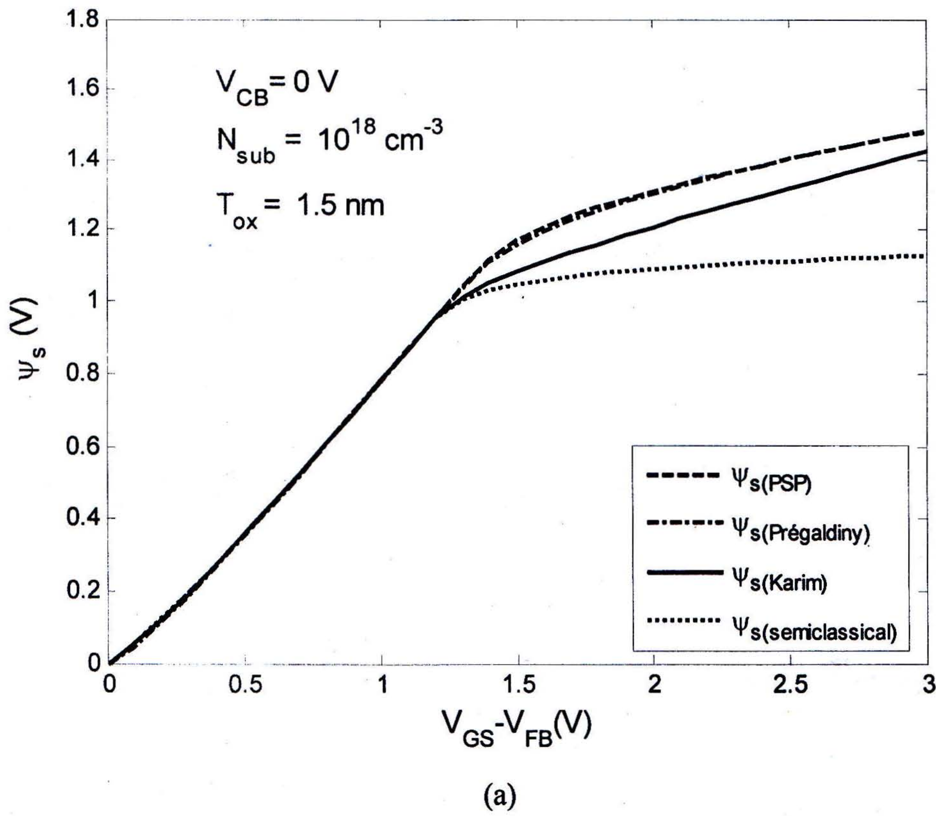

(a)

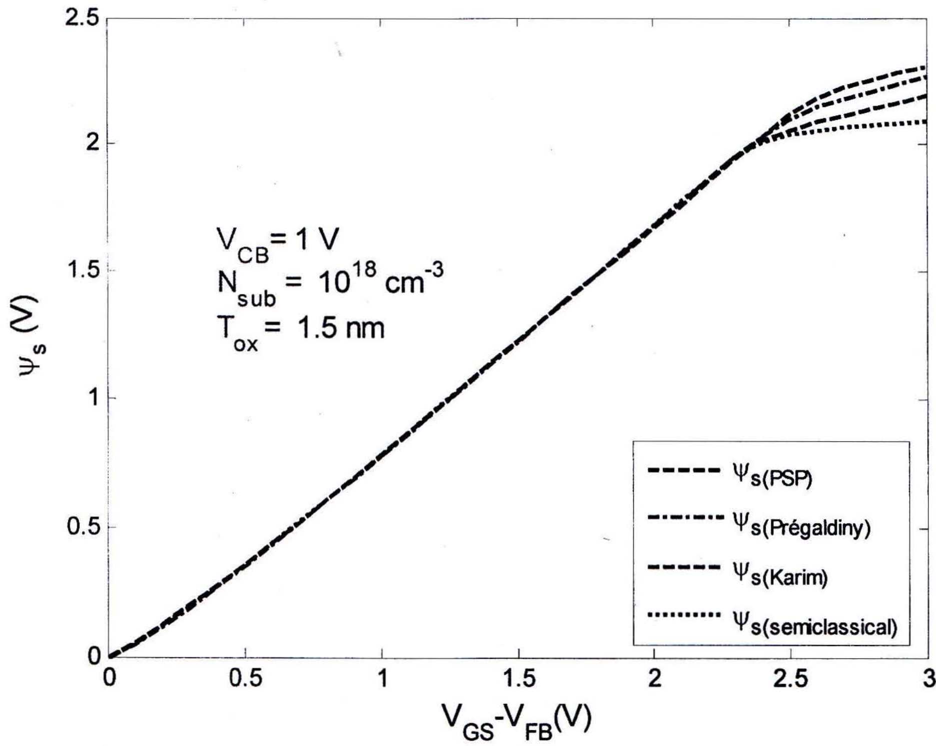

(b)

Fig.5.2 $\psi_s - V_{GS}$ characteristics

The semi-classical $I - V$ characteristic has been computed from the following drift-diffusion equations derived in chapter 2. These equations are repeated here for convenience. I_{DS1} occurs due to drift in the presence of the electric field. I_{DS2} occurs for the diffusion movement of charge.

$$I_{DS1} = \frac{W}{L} C'_{ox} \left[(V_{GB} - V_{FB})(\psi_{SL} - \psi_{SO}) - \frac{1}{2}(\psi_{SL}^2 - \psi_{SO}^2) - \frac{2}{3}\gamma(\psi_{SL}^{3/2} - \psi_{SO}^{3/2}) \right]$$

$$I_{DS2} = \frac{W}{L} C'_{ox} [\varphi_t (\psi_{SL} - \psi_{SO}) + \varphi_t \gamma \ (\psi_{SL}^{1/2} - \psi_{SO}^{1/2})]$$

The drain current, I_{DS} is the summation of the drift and diffusion currents.

$$I_{DS} = I_{DS1} + I_{DS2}$$

Due to QM effects lowering of the drain current is apparent. QM effects increase the threshold voltage and the surface potential and hence lower the current.

The QM correction approach of PSP [24] and Prégaldiny [28] has been added to the semiclassical $I - V$ characteristic to account for the QM effects. This has been compared with the Karim model [26].

Considering the case when $N_{sub} = 10^{17}\text{cm}^{-3}$ and $t_{ox} = 2.5$ nm, PSP [24] and Prégaldiny [28] is found to overestimate the increase in the threshold voltage and also the surface potential. The threshold voltages of PSP [24] and Prégaldiny [28] are 0.4 V and 0.42 V respectively, as shown in Fig. 5.3 (a) and (b). This is because it neglects the wave function penetration effect. As a result both these models also underestimate the drain current. The Karim model [26] is seen to predict the drain current more accurately as this approach is more physical and takes into account the wave function penetration effect. The Karim model [26] predicts a more accurate lower threshold voltage which is 0.35 V as shown in Fig. 5.3 (c).

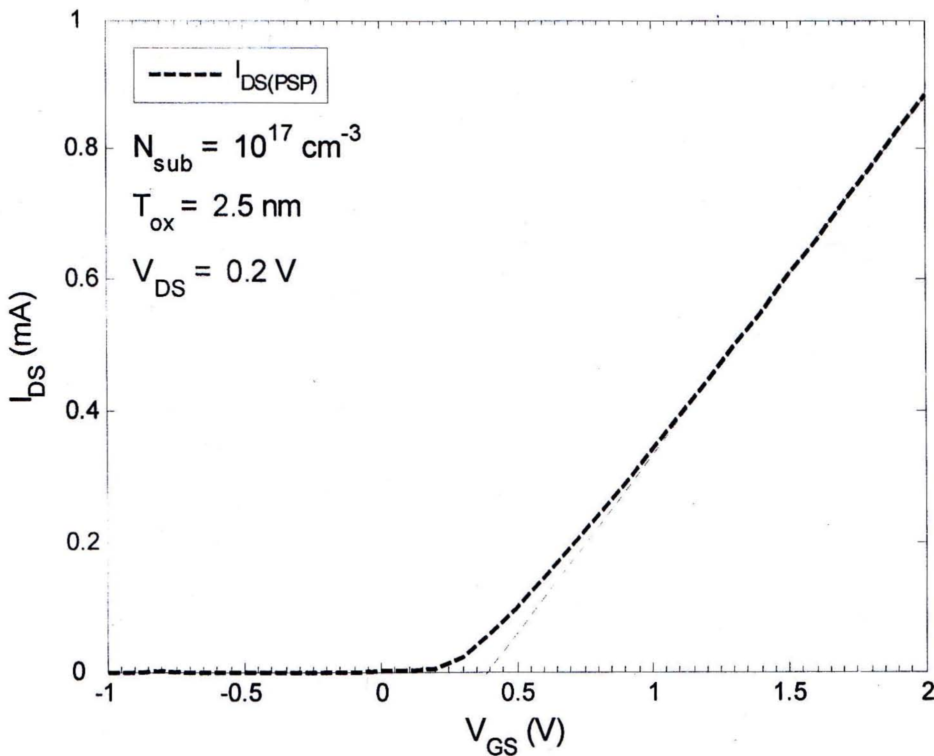

(a)

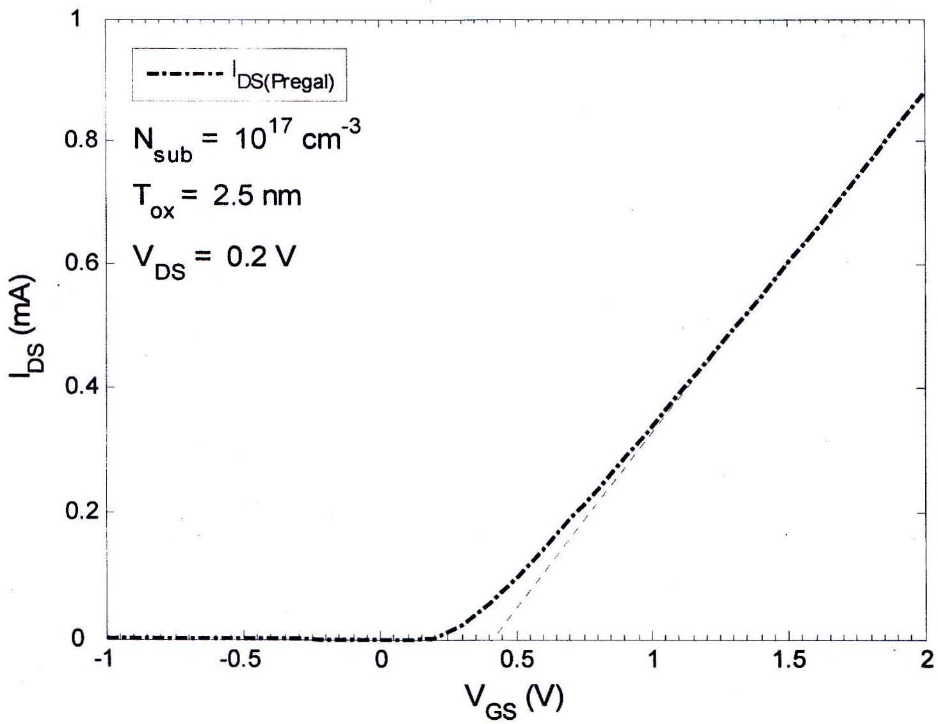

(b)

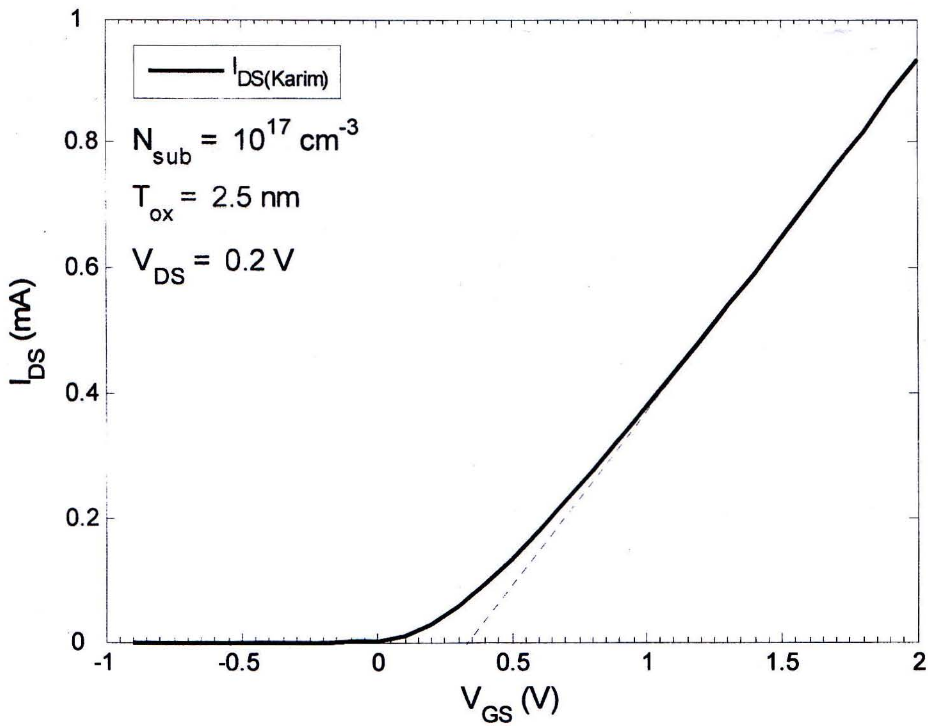

(c)

East West University LIBRARY 43, Mohakhali, C/A

Fig.5.3 $I_{DS} - V_{GS}$ characteristics for calculating threshold voltages for the three models.

Fig. 5.4 shows the $I - V$ characteristics for $N_{sub} = 10^{17}\text{cm}^{-3}$ and $t_{ox} = 2.5$ nm.

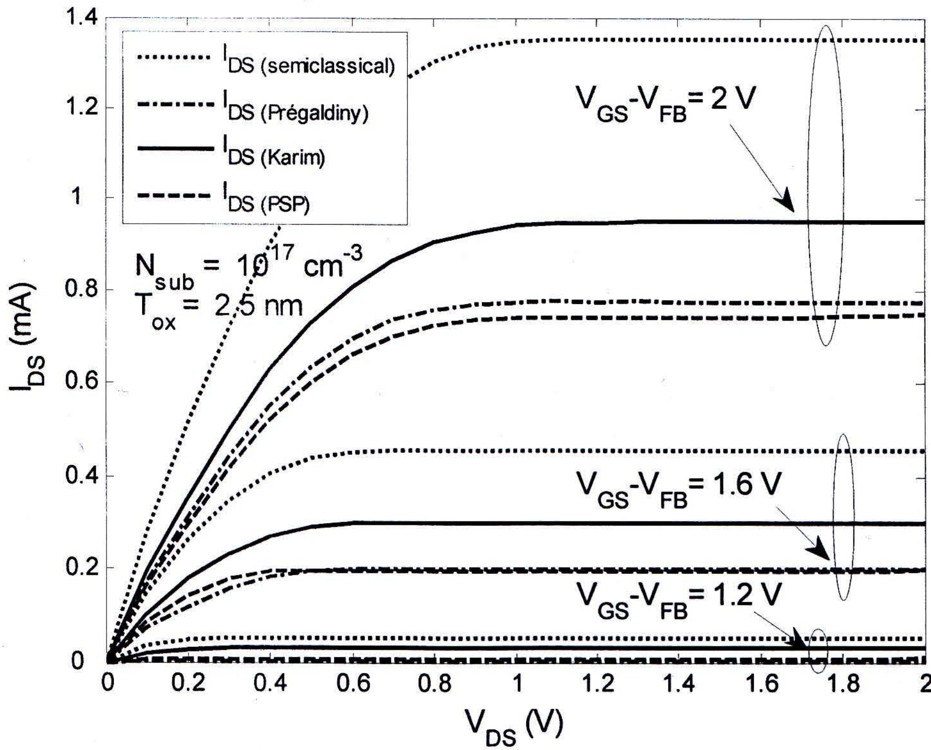

Fig.5.4 $I - V$ characteristics for $N_{sub} = 10^{17}\text{cm}^{-3}$and $t_{ox} = 2.5$ nm, $\frac{W}{L} = 5$, $C_{ox} = 0.0138$ F/cm^{-2}

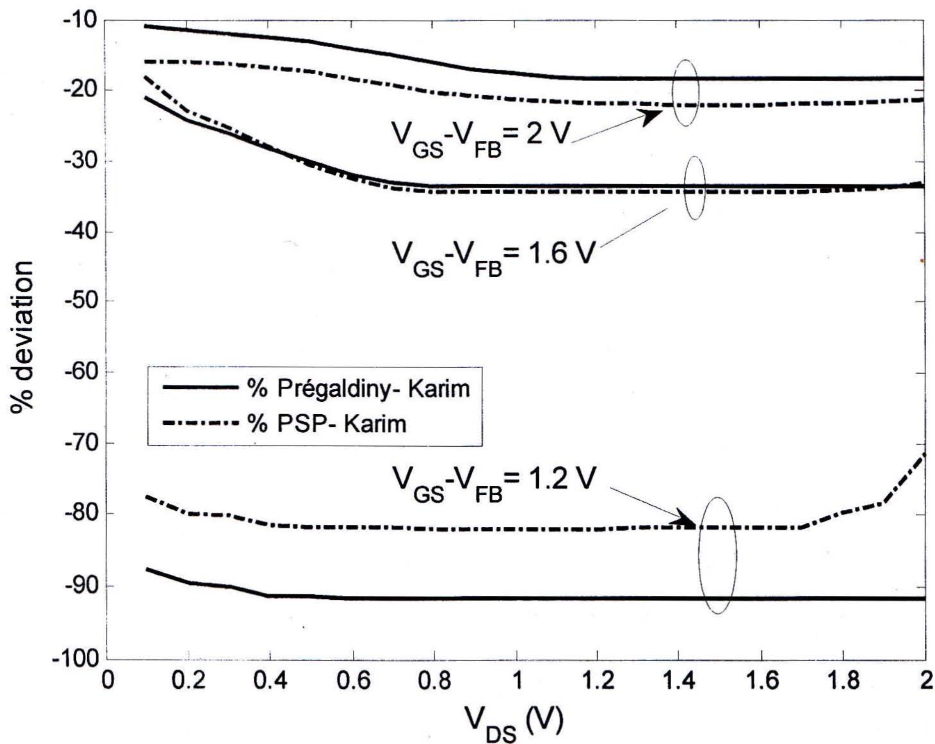

Fig.5.5 Comparison of the % deviation in drain current for $N_{sub} = 10^{17}\text{cm}^{-3}$ and $t_{ox} = 2.5$ nm

The percentage deviation of the drain current of the QM corrections of PSP [24] and Prégaldiny [28] has been calculated with respect of that of the Karim model of [26]. For $V_{GS} - V_{FB} = 1.6$ V the deviation is around 20 - 40 % and $V_{GS} - V_{FB} = 2$ V the percentage differences are around 10 – 20 %. When $V_{GS} - V_{FB} = 1.2$ V, the percentage difference of the model of PSP [24] and Prégaldiny [28] with the Karim model [26] is nearly 80 - 90%. This difference is quite noticeable.

Similarly, considering the case when $N_{sub} = 10^{18}\text{cm}^{-3}$ and $t_{ox} = 1.5$ nm the threshold voltages of PSP [24] and Prégaldiny [28] are 0.65 V and 0.55 V respectively. The Karim model [26] predicts a more accurate lower threshold voltage which is 0.5 V and hence it leads to better modeling of the drain current.

Fig. 5.6 shows the $I - V$ characteristics for $N_{sub} = 10^{18}\text{cm}^{-3}$ and $t_{ox} = 1.5$ nm.

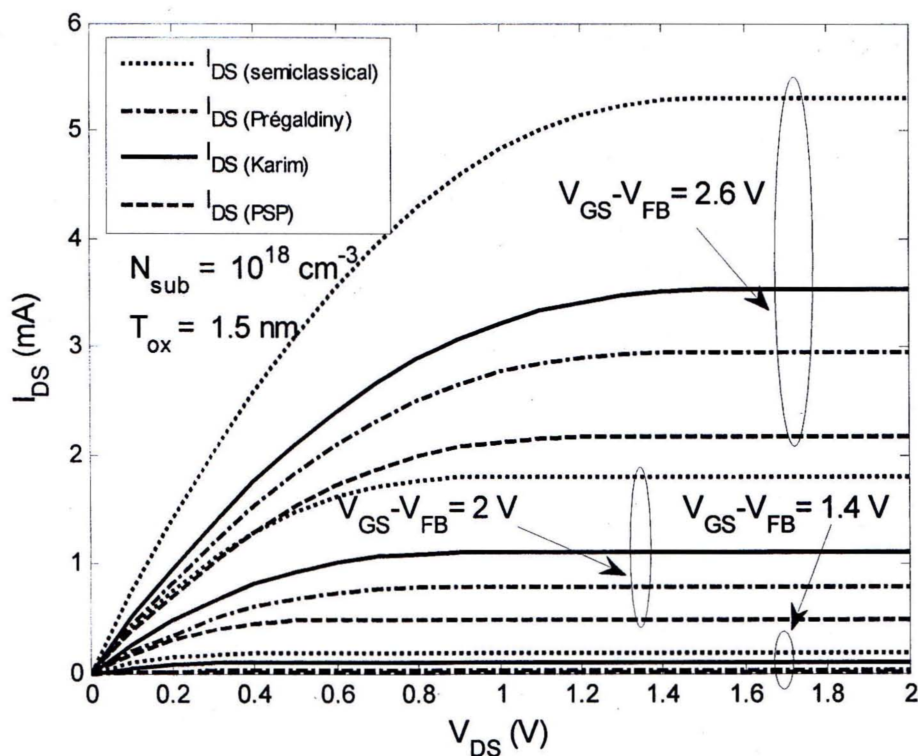

Fig.5.6 $I - V$ characteristics, here $N_{sub} = 10^{18}\text{cm}^{-3}$ and $t_{ox} = 1.5$ nm $\frac{W}{L} = 5$, $C_{ox} = 0.023$ F/cm^{-2}

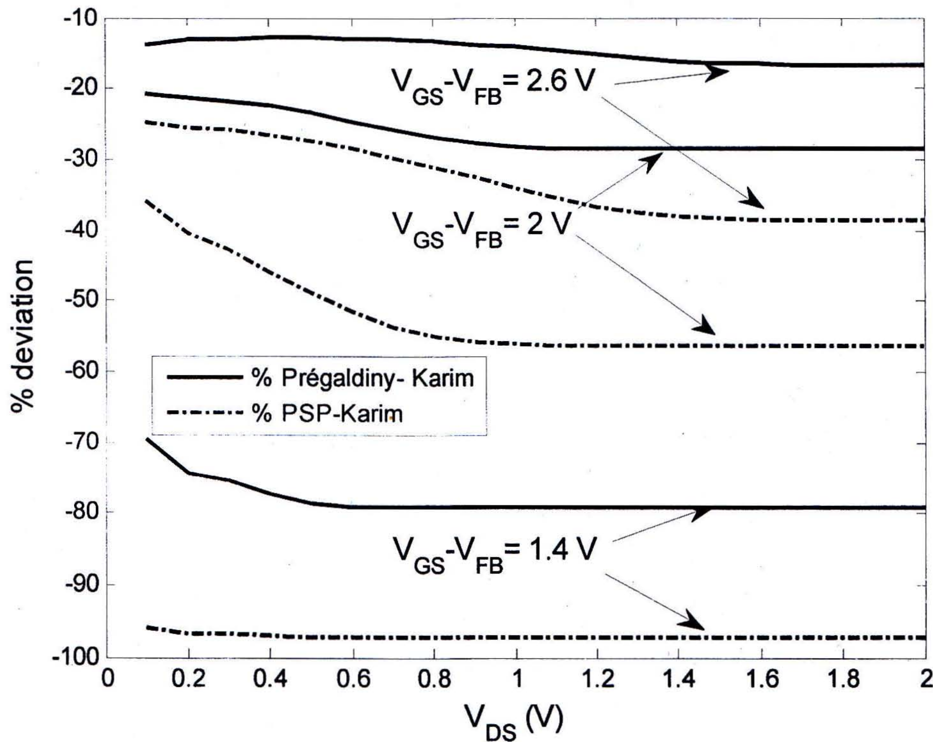

Fig.5.7 Comparison of the % deviation in drain current for $N_{sub} = 10^{18}\text{cm}^{-3}$ and $t_{ox} = 1.5$ nm

In order to obtain high concentration integration for MOS devices, it is necessary to reduce the gate oxide thickness and increase the substrate doping concentration. With increased doping density and reduced oxide thickness the QM effects increase. Here we observe that the percentage deviation in the drain current between the models also increase. The percentage difference between the model of PSP [24] and Prégaldiny [28] with the Karim model [26] is approximately is again quite remarkable, around 85 – 95% when $V_{GS} - V_{FB} =$ 1.4 V. For $V_{GS} - V_{FB} = 2$ V and $V_{GS} - V_{FB} = 2.6$ V the percentage differences are around 15 – 50 %.

5.2 Discussions

From our analysis we find that in the moderate inversion region, just above the threshold, the PSP [24] , Prégaldiny [28] models tend to miscalculate the current greatly. It shows around 80-90% deviation from the Karim model [26] in the calculation of the drain current in the region just above threshold. The PSP [24] , Prégaldiny [28] models that do not take into account the wave function penetration effect calculate a higher threshold voltage than that due to QM effects, as already shown in the previous section, 5.1. The Karim model [26] predicts a lower more accurate threshold voltage. Although the difference in current reduces as we move towards the strong inversion region, the difference is still quite remarkable, around 30-40%.

For integrated circuits with the ultra-thin oxide layer MOSFETs, the quantization effect must be included in device models to avoid large deviations from design. Analog circuit blocks rely on extremely precise matching. Even a few millivolt of mismatch can result in practically zero yields for high precision analog-to-digital and digital-to-analog converters [46].

The speed, accuracy and power consumption performances of analog circuits are linked due to the effect of mismatch on the circuit design.

As MOSFET saturation drain current is one of the most important device parameters, its modelling should be of high precision.

Hence the Karim model [26] provides a more accurate QM correction method. It is a physically based explicit model for the quantum mechanical (QM) correction to the surface potential of nanoscale metal–oxide–semiconductor (MOS) devices. The Karim model [26] is accurate over a large range of device parameters.

Chapter 6

Summary

6.1 Conclusion

In our work we have studied the impact of Quantum Mechanical correction on the drain current of surface potential based nanoscale MOSFETs. We have considered the QM correction approach of PSP [24] and Prégaldiny [28] and compared it with that of the Karim model [26]. Here we have neglected the secondary effects such as interface trap charge, parasitic charges, and short channel effects. The models PSP [24] and Prégaldiny [28] are based on bandgap widening approach and neglects the wave function penetration effect but the Karim model [26] accounts for it. Results have been derived for two sets of device parameters (doping density and oxide thickness). We have calculated the drain current for different $V_{GS} - V_{FB}$including models of [24], [26], [28] and observed the drain current characteristics. Due to QM effects, the threshold voltage increases, as a result the drain current decreases. It is observed that, the models PSP [24] and Prégaldiny [28] calculate a much lower drain current, than that actually occurs due to QM effects. This inaccuracy is more distinct in the moderate inversion region, and deviates from the drain current calculated from the Karim model [26] by approximately 80-95 %. In the strong inversion this deviation is around 10-40 %, which cannot be neglected. This discrepancy cannot be neglected when it comes to analog circuit modeling. Analog circuit blocks rely on extremely precise matching. Even a few millivolt of mismatch can result in practically zero yields for high precision analog-to-digital and digital-to-analog converters [46]. As MOSFET saturation drain current is one of the most important device parameters, its modeling should be of high precision.The Karim model [26] is a physically based, more accurate explicit model for the quantum mechanical (QM) correction to the surface potential of nanoscale metal–oxide–semiconductor (MOS) devices. It is seen that the Karim model [26] is accurate over a large range of device parameters and hence provides a better QM correction approach.

6.2 Future work

In our work so far the effects of DC $I - V$ characteristics have been studied. We have not considered the secondary effects like interface trap charge, parasitic charge on the MOSFET drain current. The effect of leakage current can be taken into account for future work for better and more accurate modeling of the drain current of nanoscale MOSFETs. The three major components of leakage current are sub-threshold leakage, gate leakage and junction leakage. Due to quantum mechanical behavior of the substrate electrons, more band bending is required to populate the lowest subband, which is at higher energy than the bottom of the conduction band. This increases the threshold voltage thereby reducing the sub-threshold current. The tunneling current increases exponentially with the decrease in the oxide thickness and the increase in the potential drop across oxide. In nanoscale devices due to higher doping at the junctions the junction leakage current becomes significant and can considerably increase the total leakage current. Effects on Radio Frequency (RF) performance, noise can also be considered for future work. The AC and noise characteristics of deep-submicron MOS device is an important issue as device size scales down and the operation frequency of CMOS circuits rises. The $1/f$ noise of MOS devices at high frequency is very low and improves strongly with scaling. The cutoff frequency, f_T, of RF MOS increases with decreasing capacitance and increasing g_m, ($f_T \approx g_m/C_g$).

References

[1] H. K. J. Ihantola and J. L. Moll, "Design theory of a surface field-effect transistor," *Solid-State Electron.*, vol. 7, no. 4, pp. 423-430, Apr. 1964.

[2] C. T. Sah, "Characteristics of the metal-oxide-semiconductor transistor," *IEEE Trans. Electron Devices*, vol. 11, no. 7, pp. 324-345, July 1964.

[3] M. B. Barron, "Low level currents in insulated gate field effect transistors, " *Solid- State Electron.*, vol. 15, no. 3, pp. 293-302, Mar. 1972.

[4] R. A. Stuart and W. Eccleston, "Leakage currents of MOS devices under surface depletion conditions," *Electron. Lett.*, vol. 8, no. 9, pp. 225-227, May 1972.

[5] Richard M. Swanson and James D. Meindl, "Ion-implanted complementary MOS transistors in low-voltage circuits," *IEEE J. Solid-State Circuits*, vol. 7, no. 2 , pp. 146-153, Apr. 1972.

[6] H. C. Pao and C. T. Sah, "Effects of diffusion current on characteristics of metal oxide (insulator)-semiconductor transistors," *Solid-State Electron.*, vol. 9, no. 10, pp. 927-937, Oct. 1966.

[7] G. Baccarani, M. Rudan, and G. Spadini, "Analytical i.g.f.e.t. model including drift and diffusion currents," *IEEE Solid-State and Electron Devices*, vol. 2, no. 2, pp. 62- 68, 1978.

[8] J. R. Brews, "A charge sheet model for the MOSFET," *Solid-State Electron.*, vol.21, no. 2, pp. 345-355, Feb. 1978.

[9] D. P. Foty, *MOSFET Modeling with SPICE – Principles and Practice*, Prentice Hall, Upper Saddle River, NJ, 1997.

[10] W. Liu, *MOSFET Models for Spice Simulation, Including BSIM3v3 and BSIM4*, John Wiley & Sons, New York, 2001.

[11] M. A. Maher and C. A. Mead, "A physical charge-controlled model for MOS transistors," in *Advanced Research in VLSI*, P. Losleben (ed.), MIT Press, Cambridge, MA, 1987.

[12] R. M. D. A. Velghe, D. B. M. Klaassen, and F. M. Klaassen. MOS Model 9, Nat.Lab. Unclassified Report NL-UR 003/94. Available upon request from Philips Research,
e-mail address: mm9 mxt@natlab.research.philips.com.

[13] M. A. Maher, *A charge-controlled model for MOS transistors*, PhD Thesis, Caltech, Pasadena, CA, 1989.

[14] Y. H. Byun, K. Lee, and M. Shur, "Unified charge control model and subthreshold current in heterostructure field effect transistors," *IEEE Electron Device Lett.*, vol. 11, no. 1, pp. 50-53, Jan. 1990.

[15] A. I. A. Cunha, M. C. Schneider and C. Galup-Montoro, "An MOS transistor model for analog circuit design", IEEE JSSC, vol. 33, no. 10, pp. 1510-1519, October 1998.

[16] C. C. Enz, F. Krummenacher, E.A. Vittoz, "A CMOS Chopper Amplifier", *IEEE Journal of Solid-State Circuits* vol. 22, no. 3, pp. 335–342, June 1987

[17] J. Watts, C. McAndrew, C. Enz, C. G. Montoro, G. Gildenblat, C. Hu, R. van Langevelde, M. M. Mattausch, R. Rios, C. T. Sah, "Advanced compact models for MOSFETs," *Proc. Workshop on Compact Modeling, Nanotech 2005*, pp. 3-12.

[18] C. Turchetti and G. Masetti, "A charge-sheet analysis of short-channel enhancement mode MOSFETs," *IEEE J. Solid State Circuits*, vol. SC-21, pp. 267–275, Apr. 1986.

[19] K. Joardar, K. K. Gullapalli, C. C. McAndrew, M. E. Burhanm, and A. Wild, "An improved MOSFET model," *IEEE Trans. Electron Devices*, vol. 45, pp. 134–148, Jan. 1998.

[20] Philips MOS Model 11, R. van Langevelde, A. J. Scholten, and D. B. M. Klaassen. (2002,Dec.).[Online].Available:http://www.semiconductors.philips.com/acrobat/other/philips models/mos-models/model11/NLUR2002802.pdf

[21] C. C. McAndrew and J. J. Victory, "Accuracy of approximations in MOSFET charge models," *IEEE Trans. Electron Devices*, vol. 49, pp. 72–81, Jan. 2002.

[22] T.-L. Chen and G. Gildenblat, "Overview of an advanced surface potential- based MOSFET model (SP)," in *Proc. Int. Conf. Modeling Simulation of Microsystems (ICMSM'02)*, San Juan, Puerto Rico, pp. 657–661, Apr. 2002.

[23] X. Gu, G. Gildenblat, G. Workman, S. Veeraraghavan, S. Shapira, and K. Stiles, "A surface potential-based extrinsic compact MOSFET model," in *Proc. Int. Conf. Modeling and Simulation of Microsystems (ICMSM'03)*, San Fransico, CA, pp. 364–367, Feb. 2003,

[24] G. Gildenblat, X. Li, W. Wu, H. Wang, A. Jha, R. van Langevelde, G. Smit, A. Scholten, and D. B. M. Klaassen, "PSP: An advanced surface-potential- based MOSFET model for circuit simulation," *IEEE Trans. Electron Devices*, vol. 53, no. 9, pp. 1979–1993, Sep. 2006

[25] M. J. van Dort, P. H. Woerlee, and A. J. Walker, "A simple model for quantisation effects in heavily-doped silicon MOSFETs at inversion conditions," *Solid State Electron.*, vol. 37, no. 3, pp. 411–414, Mar. 1994.

[26] M. A. Karim and A. Haque, “A Physically Based Accurate Model for Quantum Mechanical Correction to the Surface Potential of Nanoscale MOSFETs”, *IEEE Trans. Electron Devices*, vol. 57, no. 2, pp. 496-502, Feb.2010.

[27] R. van Langevelde, A. J. Scholten, and D. B. M. Klaassen, “Physical background of MOS model 11,” Koninklijke Philips Electron., Amsterdam, The Netherlands, Nat. Lab. Unclassified Rep. 2003/00239, Apr. 2003.

[28] F. Prégaldiny, C. Lallement, R. van Langevelde, and D. Mathiot, “An advanced explicit surface potential model physically accounting for the quantization effects in deep-submicron MOSFETs,” *Solid State Electron.*, vol. 48, no. 3, pp. 427–435, Mar. 2004.

[29] Y. Tsividis: Operation and Modeling of the MOS Transistor, 2nd edn. McGraw-Hill, New York (1999)

[30] "*International Technology Roadmap for Semiconductors (ITRS)*", Semiconductor Industry Association (SIA), 2009.

[31] S. H. Lo, D. A. Buchanan, and Y. Taur, "Modeling and characterization of quantization, polysilicon depletion, and direct tunneling effects in MOSFETs with ultrathin oxides", *IBM Journal of Research and Development*, vol. 43, no. 3, pp. 327-337, May1999.

[32] T. Yuan, D. A. Buchanan, C. Wei, D. J. Frank, K. E. Ismail, L. Shih-Hsien, G. A. Sai-Halasz, R. G. Viswanathan, H. J. C. Wann, S. J. Wind, and W. Hon-Sum, "CMOS scaling into the nanometer regime", *Proceedings of the IEEE*, vol. 85, no. 4, pp. 486-504, 1997.

[33] S. Takagi, M. Takayanagi, and A. Toriumi, "Impact of electron and hole inversion-layer capacitance on low voltage operation of scaled n- and p-MOSFET's", *IEEE Trans. Electron Devices*, vol. 47, no. 5, pp. 999-1005, 2000.

[34] M. J. van Dort, P. H. Woerlee, A. J. Walker, C. A. H. Juffermans, and H. Lifka, "Influence of high substrate doping levels on the threshold voltage and the mobility of deep-submicrometer MOSFETs", *IEEE Trans. Electron Devices*, vol. 39, no. 4, pp. 932 938, 1992.

[35] Q. Wuyun, D. M. Kim, and L. Hi-Deok, "Quantum C-V modeling in depletion and inversion: accurate extraction of electrical thickness of gate oxide in deep submicron MOSFETs", *IEEE Trans. Electron Devices*, vol. 49, no. 5, pp. 889-894, 2002.

[36] D. Vasileska, D. K. Schroder, and D. K. Ferry, "Scaled silicon MOSFETs: degradation of the total gate capacitance", *IEEE Trans. Electron Devices*, vol. 44, no. 4, pp. 584-587, 1997.

[37] L. Wang, Q. Chen, R. Murali, and J. D. Meindl, "Quantum mechanical effects on CMOS SOC performance", *SOC Conference Proc.* 2003, pp. 109-112.

[38] F. Stern, "Self-consistent results for n-type Si inversion layers," *Phys. Rev. B, Condens. Matter*, vol. 5, no. 12, pp. 4891–4899, Jun. 1972.

[39] R. Rios, N. D. Arora, C. Huang, N. Khalil, J. Faricelli, and L. Gruber, "A physical compact MOSFET model, including quantum mechanical effects, for statistical circuit design applications," in *IEDM Tech. Dig.*, Dec. 1995, pp. 937–940.

[40] G. Gildenblat, T. L. Chen, and P. Bendix, "Closed-form approximation for the perturbation of MOSFET surface potential by quantum-mechanical effects," *IEEE Electron Device Lett.*, vol. 36, no. 12, pp. 1072–1073, Jun. 2000.

[41] S. Mudanai, L.F. Register, A.F. Tasch, and S.K. Banerjee, "Understanding the effects of wave function penetration on the inversion layer capacitance of NMOSFETs," *IEEE Electron Device Letters*, vol.22, no.3, pp.145-147, 2001.

[42] F. Li, S. Mudanai, L. F. Register, and S. K. Banerjee, "A physically based compact gate *C– V* model for ultrathin (EOT ~1 nm and below) gate dielectric MOS devices," *IEEE Trans. Electron Devices*, vol. 52, no. 6, pp. 1148–1158, Jun. 2005.

[43] A. Haque and M. Z. Kauser, "A comparison of wavefunction penetration effects on gate capacitance in deep submicron n- and p-MOSFETs," *IEEE Trans. Electron Devices*, vol. 49, no. 9, pp. 1580–1587, Sep. 2002.

[44] A. E. Islam and A. Haque, "Accumulation gate capacitance of MOS devices with ultrathin high-*k* gate dielectrics: Modeling and characterization," *IEEE Trans. Electron Devices*, vol. 53, no. 6, pp. 1364–1372, Jun. 2006.

[45] UC Berkeley Device Group, Quantum Mechanical *C–V* Simulator. [Online]. Available: http://www-device.eecs.berkeley.edu/qmcv/index.shtml

[46] M. J. M. Pelgrom, H. P. Tuinhout, and M. Vertregt, "Transistor matching in analog CMOS applications", *IEDM Tech. Dig.*, pp. 915-918, 1998.

East West University LIBRARY 43, Mohakhali, C/A